10 June 2014

Science Signaling

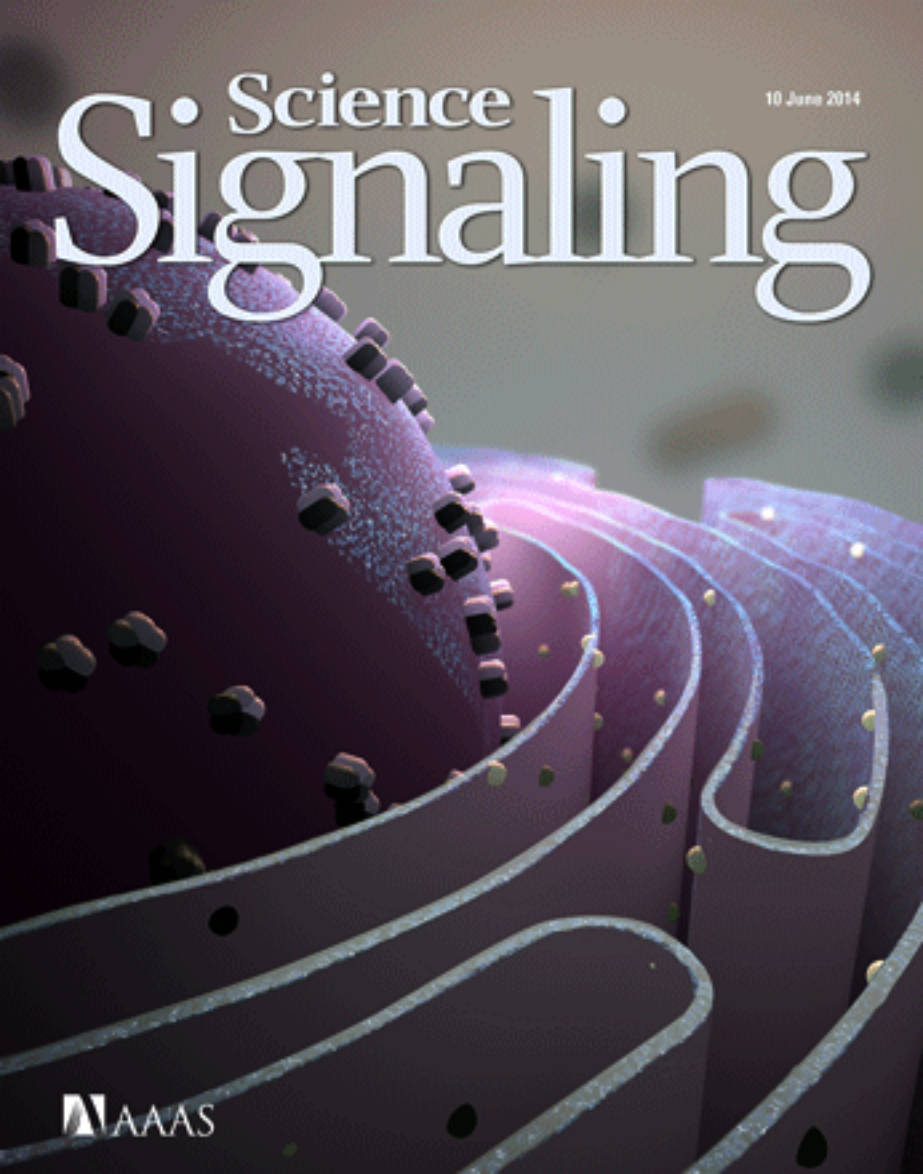

AAAS

Science Signaling
AAAS

` Interplay Between the Oxidoreductase PDIA6 and microRNA-322 Controls the Response to Disrupted Endoplasmic Reticulum Calcium Homeostasis

Jody Groenendyk, Zhenling Peng, Elzbieta Dudek, Xiao Fan, Marcin J. Mizianty, Estefanie Dufey, Hery Urra, Denisse Sepulveda, Diego Rojas-Rivera, Yunki Lim, Do Han Kim, Kayla Baretta, Sonal Srikanth, Yousang Gwack, Joohong Ahnn, Randal J. Kaufman, Sun-Kyung Lee, Claudio Hetz, Lukasz Kurgan and Marek Michalak (10 June 2014)
Science Signaling **7** (329), ra54. [DOI: 10.1126/scisignal.2004983]

Science Signaling (ISSN 1937-9145) is published weekly, except the last week in December, by the American Association for the Advancement of Science, 1200 New York Avenue, NW, Washington, DC 20005.

CELL BIOLOGY

Interplay Between the Oxidoreductase PDIA6 and microRNA-322 Controls the Response to Disrupted Endoplasmic Reticulum Calcium Homeostasis

Jody Groenendyk,[1] Zhenling Peng,[2] Elzbieta Dudek,[1] Xiao Fan,[2] Marcin J. Mizianty,[2] Estefanie Dufey,[3,4] Hery Urra,[3,4] Denisse Sepulveda,[3,4] Diego Rojas-Rivera,[3,4] Yunki Lim,[5] Do Han Kim,[5] Kayla Baretta,[1] Sonal Srikanth,[6] Yousang Gwack,[6] Joohong Ahnn,[7] Randal J. Kaufman,[8] Sun-Kyung Lee,[7] Claudio Hetz,[3,4,9] Lukasz Kurgan,[2] Marek Michalak[1]*

The disruption of the energy or nutrient balance triggers endoplasmic reticulum (ER) stress, a process that mobilizes various strategies, collectively called the unfolded protein response (UPR), which reestablish homeostasis of the ER and cell. Activation of the UPR stress sensor IRE1α (inositol-requiring enzyme 1α) stimulates its endoribonuclease activity, leading to the generation of the mRNA encoding the transcription factor XBP1 (X-box binding protein 1), which regulates the transcription of genes encoding factors involved in controlling the quality and folding of proteins. We found that the activity of IRE1α was regulated by the ER oxidoreductase PDIA6 (protein disulfide isomerase A6) and the microRNA miR-322 in response to disruption of ER Ca^{2+} homeostasis. PDIA6 interacted with IRE1α and enhanced IRE1α activity as monitored by phosphorylation of IRE1α and XBP1 mRNA splicing, but PDIA6 did not substantially affect the activity of other pathways that mediate responses to ER stress. ER Ca^{2+} depletion and activation of store-operated Ca^{2+} entry reduced the abundance of the microRNA miR-322, which increased *PDIA6* mRNA stability and, consequently, IRE1α activity during the ER stress response. In vivo experiments with mice and worms showed that the induction of ER stress correlated with decreased miR-322 abundance, increased *PDIA6* mRNA abundance, or both. Together, these findings demonstrated that ER Ca^{2+}, PDIA6, IRE1α, and miR-322 function in a dynamic feedback loop modulating the UPR under conditions of disrupted ER Ca^{2+} homeostasis.

INTRODUCTION

The endoplasmic reticulum (ER) is involved in the production of newly synthesized secretory and membrane proteins, where several mechanisms control proper folding and posttranslational modifications of these proteins. Many different intrinsic and extrinsic factors may disrupt ER homeostasis, leading to the activation of ER stress coping responses and multiple corrective strategies (*1*). A strategy to restore homeostasis is the activation of the unfolded protein response (UPR) (*2*, *3*). The UPR is a dynamic signal transduction pathway that reduces unfolded protein load by attenuating protein synthesis, increasing protein chaperone production, and augmenting ER-associated degradation (ERAD) and autophagy (*3*–*6*). The UPR signals through activating transcription factor 6 (ATF6); inositol-requiring enzyme 1α (IRE1α), a bifunctional protein kinase and endoribonuclease; and double-stranded RNA–activated protein kinase–like ER kinase (PERK), which phosphorylates and inactivates eukaryotic translation initiation factor 2 on the α subunit (eIF2α). These sensors are maintained in an inactive state through interaction with the ER chaperone immunoglobulin binding protein (BiP) (*4*–*6*). As misfolded proteins in the ER accumulate, BiP binds to them to prevent aggregation and in the process is released from the sensors, permitting their activation. Each sensor activates downstream factors that transcriptionally regulate genes that enable adaptation to stress or trigger the induction of apoptosis. For example, activated IRE1α undergoes autophosphorylation and oligomerization, leading to the conformational activation of the endoribonuclease domain, which splices the mRNA encoding the transcription factor XBP1 (X-box binding protein 1). This processing event removes a 26-base intron in the coding region that changes the reading frame, producing the transcription factor spliced XBP1 (XBP1s) (*7*). XBP1s binds to ER stress elements (ERSEs) and UPR elements (UPREs) to transcriptionally activate genes encoding proteins involved in protein folding, transport, and ERAD (*8*, *9*). Depending on the intensity and the duration of the stress stimuli, UPR signaling events may trigger cell adaptation or the induction of apoptosis through complementary mechanisms including BCL-2 family members, microRNAs (miRNAs), and other factors (*1*, *10*, *11*).

Depletion of ER Ca^{2+} stores results in the activation of store-operated Ca^{2+} entry (SOCE), an important Ca^{2+} signaling pathway (*12*). Prolonged ER Ca^{2+} depletion, in addition to the induction of SOCE, is also a potent inducer of ER stress, resulting in disrupted ER homeostasis, accumulation of misfolded proteins, and activation of the three branches of the UPR (*1*, *6*). Fine-tuning the UPR response is fundamental to determine whether cells survive or undergo apoptosis under ER stress, and increasing evidence indicates that the activity of the UPR sensors may be modulated

[1]Department of Biochemistry, University of Alberta, Edmonton, Alberta T6G 2S7, Canada. [2]Department of Electrical and Computer Engineering, University of Alberta, Edmonton, Alberta T6G 2V4, Canada. [3]Biomedical Neuroscience Institute, Faculty of Medicine, University of Chile, Santiago, Chile. [4]Program of Cellular and Molecular Biology, Institute of Biomedical Sciences, University of Chile, Santiago, Chile. [5]College of Life Sciences, Gwangju Institute of Science and Technology (GIST), Gwangju 500-712, Korea. [6]Department of Physiology, University of California, Los Angeles, Los Angeles, CA 90095, USA. [7]Department of Life Science, BK21 PLUS Life Science for BDR team, The Research Institute of Natural Sciences, Hanyang University, Seoul 133-791, Korea. [8]Degenerative Disease Research Program, Center for Neuroscience, Aging, and Stem Cell Research, Cancer Center, Sanford Burnham Medical Research Institute, La Jolla, CA 92037, USA. [9]Neurounion Biomedical Foundation, Santiago, Chile.
*Corresponding author. E-mail: marek.michalak@ualberta.ca

through the direct binding of specific regulators (*6*). Here, we focused on identifying ER stress coping responses induced by disruption of the ER homeostasis by depletion of ER Ca^{2+} stores. We used a small interfering RNA (siRNA) library screen combined with deep sequencing miRNA analysis to identify factors that mediate UPR modulation. We discovered that silencing of the gene encoding PDIA6, an ER-resident oxidoreductase, affected ER Ca^{2+} depletion–dependent activation of the IRE1α signaling branch. Deep sequencing analysis identified miR-322 as one of the miRNAs that were significantly decreased in abundance after ER Ca^{2+} store depletion–induced ER stress. We also showed that Ca^{2+} store depletion and SOCE activation–dependent activation of IRE1α by PDIA6 were affected by Ca^{2+} and miR-322. The PDIA6 gene was a target of miR-322, and miR-322 abundance was sensitive to changes in ER and cytosolic Ca^{2+} concentrations. This work identified PDIA6 as a component of the UPR and demonstrated interplay between ER and cytosolic Ca^{2+}, PDIA6, IRE1α, and miR-322 as a part of a coping mechanism activated by disrupted ER Ca^{2+} homeostasis and activation of SOCE as an adaptive response to cope with ER stress.

RESULTS

An siRNA screen identifies a role for PDIA6 in Ca^{2+} store depletion–induced UPR

To identify the molecular factors involved in the ER luminal Ca^{2+} depletion–dependent modulation of the UPR, we performed a genome-wide siRNA screen for genes required for IRE1α activation or inactivation. We used NIH-3T3 cells transfected with the pRL-IXFL XBP1 mRNA splicing reporter plasmid (fig. S1) (*13*).

To identify genes required for Ca^{2+} store depletion–induced ER stress, reporter cells transfected with the siRNA library were treated with thapsigargin, a SERCA (sarcoplasmic/endoplasmic reticulum Ca^{2+} ATPase) inhibitor, to induce ER Ca^{2+} depletion and activation of SOCE (*14*). The library included internal controls such as a scrambled siRNA, an siRNA targeting IRE1α as a negative control, and an siRNA targeting BiP as a positive control for ER stress (fig. S2). Analysis of about 6600 genes identified 5 gene candidates whose knockdown produced the highest increase and 4 genes whose knockdown produced the greatest decrease in IRE1α reporter activity in response to ER stress due to ER Ca^{2+} store depletion (Table 1). One of the genes in the latter group was *PDIA6*, which encoded an ER luminal oxidoreductase. This protein was selected for further analysis on the basis of its subcellular localization and statistical analysis.

We validated a role for PDIA6 in ER stress responses by transfecting the reporter cell line with siRNA directed against PDIA6 (fig. S3A). Cell growth was not affected by siRNA transfection (fig. S2D). Quantitative polymerase chain reaction (qPCR) and Western blot analyses confirmed that the siRNA was effective in silencing PDIA6 at the mRNA and protein levels (up to 95%) under both control and thapsigargin-treated conditions (fig. S3, A and B). PDIA6 abundance can be increased by pharmacological induction of ER stress (*15*) or during cardiac ischemia (*16*); therefore, we also monitored PDIA6 mRNA abundance under ER stress conditions. Thapsigargin stimulation led to a fourfold increase in PDIA6 mRNA abundance, which was prevented by siRNA-dependent silencing (fig. S3B). In our system, thapsigargin treatment triggered a 20-fold increase in the activity of the XBP1 reporter (Fig. 1A). Under these conditions, the PERK pathway was also activated as measured by phosphorylation of eIF2α, confirming that thapsigargin activated other UPR pathways (fig. S4). As expected, silencing of the ER chaperone BiP (fig. S3A) resulted in robust induction of reporter activity under unstimulated conditions (Fig. 1A), and silencing of IRE1α (fig. S3A) caused a fourfold reduction in reporter activity with thapsigargin treatment (Fig. 1A). Silencing of PDIA6 significantly reduced IRE1α reporter activity in response to thapsigargin (Fig. 1C), to a similar extent as silencing of IRE1α (Fig. 1A). This reduction in IRE1α reporter activity was recapitulated by transfection of a PDIA6 siRNA pool as well as with four independent PDIA6-specific siRNAs (fig. S3, C and D). Next, we used tunicamycin, an inhibitor of N-linked protein glycosylation (*17*) that induces protein misfolding and activates XBP1 splicing. Tunicamycin did not affect the activity of the IRE1α reporter activity at the concentration and time point tested (Fig. 1B), suggesting that PDA6 may specifically regulate IRE1α under conditions of ER Ca^{2+} depletion.

Next, we asked whether PDIA6 affected splicing of endogenous XBP1 mRNA. Endogenous XBP1 was efficiently spliced in cells in response to thapsigargin (Fig. 1C). Because the XBP1 amplicon fragment in the spliced intron contains a unique Pst I restriction site, we expected that Pst I would digest the unspliced XBP1 but not the spliced variant of XBP1, which would enable quantitative analysis of the splicing event (Fig. 1C). Total XBP1 mRNA abundance was not affected in PDIA6-silenced and thapsigargin-treated cells (Fig. 1D). Using qPCR, we confirmed that knocking down PDIA6 reduced the splicing of endogenous XBP1 mRNA in response to thapsigargin treatment (Fig. 1E). Therefore, we concluded that silencing of PDIA6 attenuates IRE1α signaling as measured by XBP1 mRNA splicing in response to ER Ca^{2+} depletion.

Because the PDIA6 gene contains several ERSEs in its proximal promoter region, we tested whether the PDIA6 gene was sensitive to thapsigargin-induced ER stress. Thapsigargin treatment induced an increase in the mRNA abundance of PDIA6 but not that of PDIA7, another ER-associated oxidoreductase (Fig. 1F). PDIA6 mRNA was increased in cells treated with thapsigargin, tunicamycin, brefeldin A, and the ER luminal Ca^{2+} chelator

Table 1. Gene candidates identified by a genome-wide siRNA screen.

RefSeq	Gene ID	Gene symbol	Ratio firefly/*Renilla*	IRE1α reporter activity	
				Normalized value	High or low
NM_145360	319554	Idi1	0.173948	8.71×10^{-6}	Low
NM_027959	71853	PDIA6	0.173993	3.68×10^{-7}	Low
NM_145561	231382	BC020151	0.174441	3.75×10^{-6}	Low
NM_007898	13595	Ebp	0.195196	5.17×10^{-6}	Low
NM_008323	15929	Idh3g	0.376557	0.999998	High
NM_172780	236794	Slc9a6	0.389342	0.999976	High
NM_019420	54218	B3galt4	0.395039	1.0	High
NM_130864	113868	Acaa1	0.444224	0.99983	High
NM_007515	11989	Slc7a3	0.541056	0.999997	High

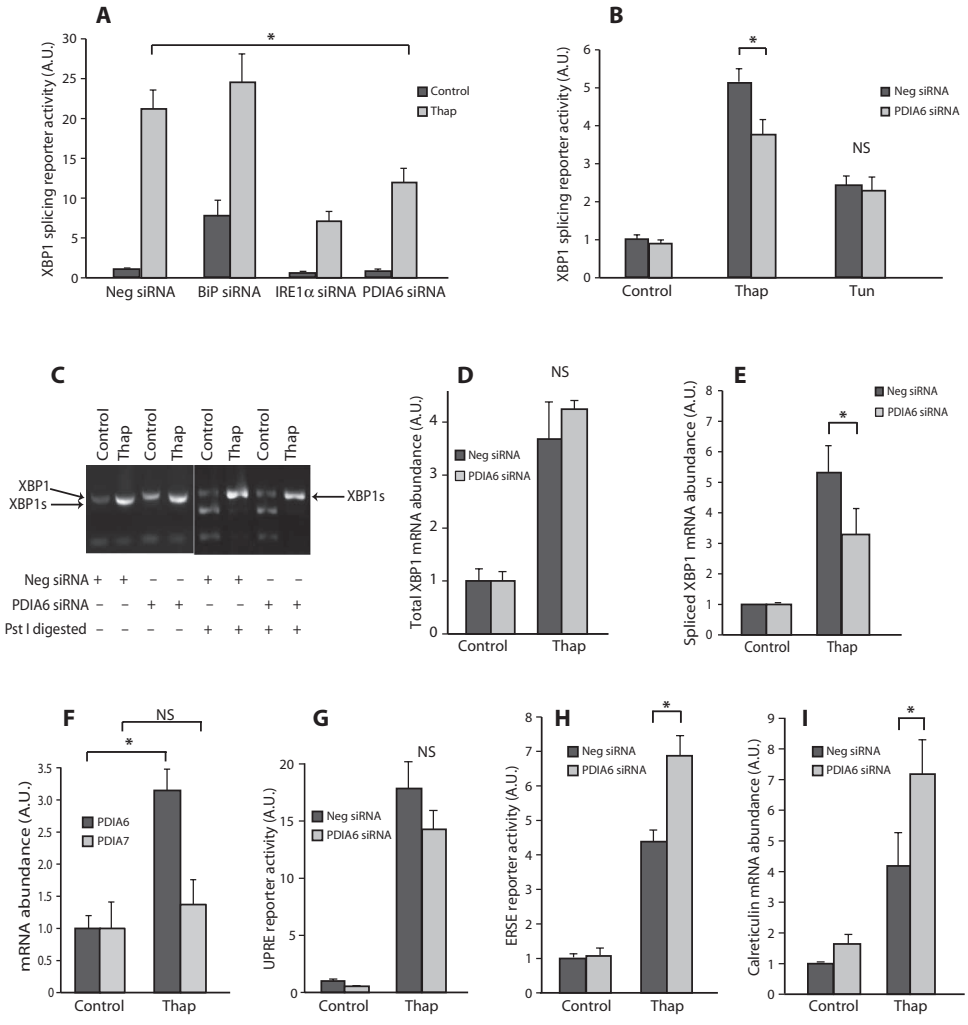

Fig. 1. Silencing of PDIA6 modulates IRE1α activity. (**A** and **B**) NIH-3T3 cells were transfected with XBP1 splicing reporter and siRNA directed against PDIA6, BiP, IRE1α, or negative scrambled control (Neg) and treated with thapsigargin (Thap) (A and B) or tunicamycin (Tun) (B). In (A), *P = 0.002598. In (B), *P = 0.002598. NS, not significant. (**C**) RT-PCR analysis of XBP1 splicing in control cells and cells treated with siRNA against PDIA6. Right panel: PCR products were digested with Pst I. (**D** and **E**) qPCR analysis of total XBP1 (D) and XBP1s (E) in control and PDIA6-silenced cells treated with thapsigargin. P = 0.0124. (**F**) qPCR analysis of PDIA6 and PDIA7 in control and thapsigargin-treated cells. (**G**) UPRE splicing reporter activity in NIH-3T3 fibroblasts transfected with PDIA6 siRNA. (**H**) ERSE splicing reporter activity in NIH-3T3 fibroblasts transfected with PDIA6 siRNA. *P = 0.004284. (**I**) NIH-3T3 fibroblasts were transfected with PDIA6 siRNA, followed by treatment with thapsigargin. *P = 0.0098. All data are representative of more than three biological replicates. NS, not significant.

TPEN [*N*,*N*,*N*′,*N*′-tetrakis(2-pyridylmethyl)ethylenediamine], but not when ER stress was induced by oxidative stress through the addition of dithiothreitol (DTT) or treatment with cyclosporin A (CSA) or staurosporine (fig. S5). These results suggest that PDIA6 mRNA abundance is selectively regulated by specific ER stress stimuli.

PDIA6 differentially affects the IRE1α and ATF6 pathways

Next, we tested whether PDIA6 silencing influenced other branches of the UPR using the UPRE and ERSE reporters. The UPRE reporter contains an UPRE that responds to the transcriptional activities of XBP1 and ATF6α (*18*). The ERSE reporter contains multiple ERSEs that report ATF6 transcriptional activity (*19*). ATF6 exhibits low affinity for the UPRE but high affinity for the ERSE, whereas XBP1 has high affinity for the UPRE but low affinity for the ERSE (*19*). The induction of the UPRE reporter in response to thapsigargin was not affected by PDIA6 silencing under these conditions (Fig. 1G). In contrast, the response of the ERSE to thapsigargin was significantly increased upon PDIA6 silencing (Fig. 1H). Furthermore, these conditions also increased the expression of the gene encoding calreticulin (Fig. 1I), a Ca^{2+}-sensitive ERSE-responsive gene (*20*). These data suggest that in the absence of PDIA6, Ca^{2+} store depletion resulted in activation of the ATF6 pathway. Next, we tested the effect of PDIA6 on the PERK pathway by analyzing the phosphorylation of Ser^{51} in eIF2α. Western blot analysis showed that thapsigargin treatment induced phosphorylation of Ser^{51} in eIF2α, which was not affected by PDIA6 silencing with the time point and concentration of thapsigargin used (fig. S4). Combined with the XBP1 reporter data, we concluded that PDIA6 silencing did not affect the PERK pathway but suppressed IRE1α activity and increased ATF6 activity in response to ER Ca^{2+} store depletion–induced ER stress.

PDIA6 forms complexes with BiP and IRE1α

We hypothesized that PDIA6 could regulate UPR signaling through physical interactions with ER stress sensors and/or ER luminal modulators. As previously reported (*21*, *22*), BiP coimmunoprecipitated with PDIA6 (Fig. 2A). PDIA6 also coimmunoprecipitated with IRE1α (Fig. 2, B and C), and PDIA6-IRE1α complex formation did not appear to be altered when immunoprecipitation was carried out from cells treated with thapsigargin (Fig. 2, B and C). We also showed that calreticulin, another ER luminal resident protein, was not present in BiP, PDIA6, or IRE1α immunocomplexes (Fig. 2D).

Three additional techniques provided evidence for a potential interaction between PDIA6 and IRE1α. His-tagged IRE1α ER luminal domain (IRE1-NLD) pulled down PDIA6 in the absence or presence of ER stress (fig. S6A). Using surface plasmon resonance (BIACore) and thermophoresis, we showed that PDIA6, but not calreticulin, tightly bound to the immobilized IRE1α with a relatively high affinity (K_D) of about 22 nM (fig. S6, B and E). Thus, PDIA6 could directly associate with the ER luminal domain of IRE1α with high affinity and form a stable complex.

Because PDIA6 is an ER luminal oxidoreductase, we considered whether Cys^{109}, Cys^{148}, and Cys^{332} in the ER luminal portion of IRE1α could be involved in binding to PDIA6. Cys^{109} and Cys^{148} are highly conserved in the IRE1α proteins (*23*). We generated C109A, C148A, and

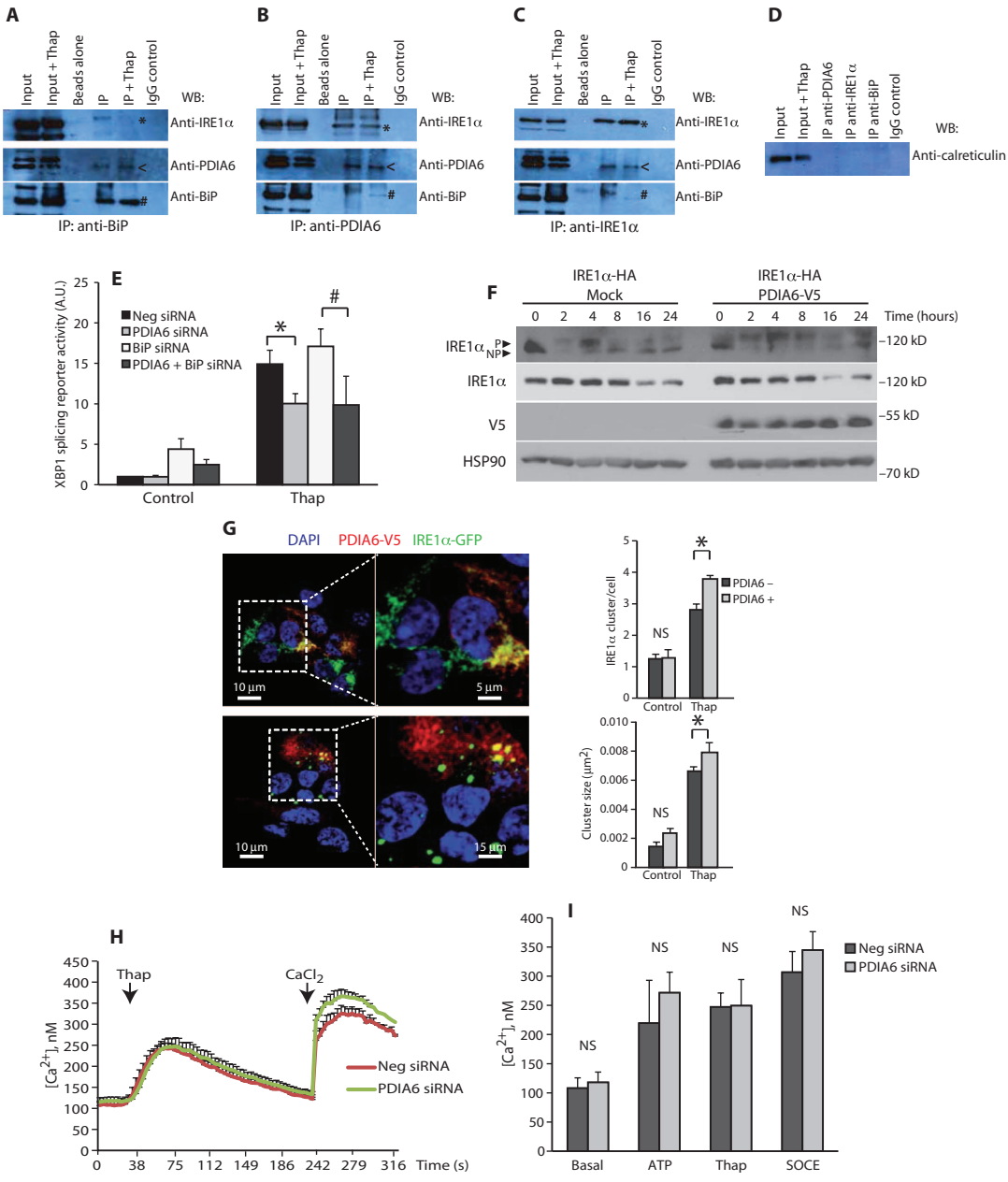

Fig. 2. PDIA6 interacts with BiP and IRE1α and controls IRE1α activity. (A to C) Top blots: To detect associations of IRE1 with proteins involved in ER stress responses, immunoprecipitations (IP) with anti-BiP, anti-PDIA6, or anti-IRE1α were performed in COS-1 cells expressing IRE1-NLD, and immunoprecipitates were immunoblotted with IRE1α antibodies. Middle and bottom blots: Immunoprecipitations with anti-BiP, anti-PDIA6, or anti-IRE1α were performed in NIH-3T3 fibroblasts, and immunoprecipitates were immunoblotted with anti-PDIA6 or anti-BiP. *, location of IRE1-NLD protein band; <, location of PDIA6 protein band; #, location of BiP protein band. (D) Immunoprecipitations with anti-BiP, anti-PDIA6, or anti-IRE1α were performed in NIH-3T3 fibroblasts, and immunoprecipitates were immunoblotted with anti-calreticulin. Data in (A) to (D) are representative of more than three biological replicates. (E) Activity of the XBP1 splicing reporter in NIH-3T3 fibroblasts transfected with siRNA for PDIA6, BiP. $^{*}P = 0.00176$; $^{\#}P = 0.04988$. Data are representative of more than three biological replicates. (F) Phosphorylation of IRE1α-HA (hemagglutinin) was analyzed by a Phostag assay in HEK293 cells expressing IRE1α-HA or IRE1α-HA and PDIA6-V5. P, phosphorylated protein band; NP, nonphosphorylated protein band. Total abundance of IRE1α-HA and PDAI-V5 proteins was analyzed by Western blot. Data are representative of three biological replicates. (G) HEK293 cells expressing IRE1-GFP were transiently transfected with expression vector encoding PDIA6-V5 or control vector (control) and treated with thapsigargin (Thap). Left panel: IRE1α-GFP–positive clusters were analyzed by immunofluorescence in cells expressing PDIA6-V5. Right panel: IRE1α clusters per cell and cluster size. For clusters per cell, $P = 0.0417$; for cluster size, $P = 0.0274$. A representative experiment of three independent experiments is presented. Sixty cells were analyzed for each independent experiment. (H and I) Ca^{2+} measurements in cells with silenced PDIA6. SOCE was initiated by the addition of $CaCl_2$. Data are representative of more than three biological replicates.

C332A mutations to create the triple IRE1-NLD mutant (C109,148,332A-IRE1-NLD). PDIA6 binding to the C109,148,332A-IRE1-NLD mutant was greatly reduced as assessed by surface plasmon resonance analysis (fig. S6C), suggesting that cysteine residues were involved in the binding of PDIA6 to IRE1α. In addition, surface plasmon resonance indicated that PDIA6 did not interact with wild-type IRE1-NLD domain treated with *N*-ethylmaleimide (NEM), which alkylates cysteine thiols, thereby irreversibly blocking the cysteines (fig. S6D). Together, these results suggested that cysteine residues in the IRE1α ER luminal domain were required for binding to PDIA6. Furthermore, binding of PDIA6 to IRE1-NLD was abolished in the presence of EGTA (fig. S6D), indicating that under BIACore conditions, there was a requirement for Ca^{2+} for the PDIA6-IRE1-NLD interaction. Finally, MicroScale Thermophoresis (MST) showed that PDIA6 bound IRE1-NLD with a similar affinity (20 nM) to that determined by surface plasmon resonance (fig. S6, B and E). Together, these results indicated that PDIA6 formed complexes with both BiP and IRE1α, and these interactions may be at least partially responsible for PDIA6-dependent effects on IRE1α activity.

Considering that PDIA6 and BiP form complexes, we asked whether PDIA6 directly affected the activity of BiP toward the activation of IRE1α-mediated ER stress responses. The increase in IRE1α reporter activity was reduced by silencing of PDIA6 and enhanced by silencing of BiP (Fig. 2E). When both genes were silenced, PDIA6 silencing blunted the increase in the ER stress that was caused by BiP silencing (Fig. 2E). Thus, in the absence of BiP, IRE1α activity was modulated by the silencing of PDIA6, but BiP was not necessary for PDIA6-dependent regulation of IRE1α.

PDIA6 regulates the inactivation of IRE1α

Because the effects of PDIA6 were observed in cells exposed to prolonged treatments with thapsigargin, we monitored the early-stage kinetics of phosphorylation of IRE1α. Time course experiments indicated that the early increase in the phosphorylation of IRE1α in thapsigargin-treated wild-type cells was transient (Fig. 2F). In cells overexpressing PDIA6, phosphorylation of IRE1α was sustained upon thapsigargin treatment, even up to 24 hours of treatment (Fig. 2F). Autophosphorylated and dimerized IRE1α form large clusters that enhance its activity (*24*). In a cell line expressing doxycycline-inducible IRE1α–GFP (green fluorescent protein) (*24*), the number and size of IRE1α clusters in cells were increased by the expression of PDIA6-V5 and treatment with thapsigargin (Fig. 2G). We concluded that increased PDIA6 abundance promoted the sustained activation of IRE1α signaling.

To process the mRNA encoding for XBP1, the ribonuclease (RNase) activity of IRE1α mediates the rapid degradation of a subset of mRNAs that encode ER membrane–associated or secreted proteins, a process referred to as regulated IRE1α-dependent decay (RIDD) (*25*–*27*). We measured the mRNA abundance of *col6* and *scara*, which are IRE1α RIDD substrates (fig. S7). As expected, wild-type cells exposed to the thapsigargin-induced ER stress exhibited a time-dependent decay of *col6* and *scara* mRNA (fig. S7). In the early phase of IRE1α activation, PDIA6 overexpression in human embryonic kidney (HEK) 293T cells resulted in increased decay of *scara* mRNA, but not of *col6* mRNA (fig. S7). Together, these results suggest that increased PDIA6 abundance may affect different IRE1α signaling outputs by modulating the kinetics of IRE1α activation.

PDIA6 does not disrupt ER Ca^{2+} homeostasis

PDIA6 resides in the lumen of the ER and contains acidic amino acid residues near the C terminus that may be involved in Ca^{2+} binding that could enable PDIA6 to play a role in buffering ER luminal Ca^{2+} (*28*). We asked whether PDIA6 affected Ca^{2+} buffering of the ER and consequently ER Ca^{2+} homeostasis. In cells treated with thapsigargin or adenosine triphosphate (ATP) to induce Ca^{2+} release from the ER, PDIA6 silencing did not alter the amount of Ca^{2+} released from the ER or the amount of SOCE (Fig. 2, H and I). These results suggest that PDIA6 modulated IRE1α activity through a direct interaction between the two proteins, rather than by directly altering ER Ca^{2+} homeostasis.

PDIA6 is a target for miR-322

Thapsigargin-dependent activation of the UPR by Ca^{2+} store depletion involves changes in miRNA abundance (*29*); therefore, we carried out deep sequencing analysis of thapsigargin-treated NIH-3T3 cells and identified 13 miRNAs showing differential expression. Eight of these miRNAs showed increased expression (miR-217, miR-216, miR-217*, miR-216b, miR-92a-1, miR-708, miR-1937a, and miR-101b), whereas five exhibited decreased expression (miR-671-5p, miR-503, miR-669f-3p, miR-322, and miR-143) in response to thapsigargin treatment (fig. S8). We used multiple target prediction programs, including TargetScan (*30*, *31*), DIANAmicroT (*32*), and RepTar (*33*), to generate a list of candidate transcripts with putative miRNA binding sites. Using Ingenuity Pathways Analysis (IPA), we determined that each miRNA had the potential to target different cellular pathways. Direct comparison of the two screens (fig. S9) revealed an overlap between miRNA targets and the top candidates in the siRNA library screen. Bioinformatics analysis indicated that miR-322 (miR-424 in the human miRNA database) might target the PDIA6 gene.

qPCR analysis of thapsigargin-treated NIH-3T3 cells showed that miR-322 abundance was reduced over 60% by depletion of Ca^{2+} stores (Fig. 3A), thus confirming the deep sequencing results. To determine whether PDIA6 was a target for miR-322, we used chemically synthesized miRNA "mimics" (*34*) to ectopically increase miR-322 abundance (Fig. 3B). The miR-322 mimic decreased the activity of the IRE1α reporter (Fig. 3C) in a manner that was dependent on ER Ca^{2+} depletion. It also decreased the mRNA and protein abundance of PDIA6 (Fig. 3, D and E). Next, we measured miR-322–mediated translational repression of PDIA6 mRNA using a luciferase reporter containing the predicted miR-322 targeting the PDIA6 3′ untranslated region (3′UTR) sequence. Luciferase reporter activity was decreased by transfection of the miR-322 mimic and increased by transfection of anti–miR-322 (Fig. 3F). These results suggested that miR-322 targeted the 3′UTR of PDIA6 mRNA.

IRE1α can act as an endoribonuclease for specific miRNAs (*35*), and many miRNAs are regulated by the UPR (*36*). Therefore, we tested whether the abundance of miR-322 depended on IRE1α. miR-322 abundance was increased 2.5-fold in IRE1α-deficient cells compared with control cells (Fig. 3G), suggesting that IRE1α affected miR-322 abundance. It remains to be determined whether miR-322 abundance is directly controlled by the RNase activity of IRE1α or through downstream signaling responses. Together, these findings indicated that miR-322 abundance was sensitive to ER Ca^{2+} depletion–induced ER stress and modulated by IRE1α, thereby directly affecting the downstream expression of PDIA6 mRNA at the transcriptional and translational levels.

miR-322 abundance is regulated by ER Ca^{2+} depletion and activation of SOCE

Although miR-322 abundance was robustly reduced in cells treated with thapsigargin, it was not significantly affected in cells treated with CSA, DTT, tunicamycin, or brefeldin A (Fig. 3H). We concluded that miR-322 abundance was not affected by ER stress induced by redox or folding environment changes but that it was sensitive to ER stress induced by thapsigargin.

To examine whether SOCE activity and, consequently, changes in the cytosolic Ca^{2+} concentration in thapsigargin-treated cells also played a role in the regulation of miR-322 abundance, we used cells deficient in ORAI1,

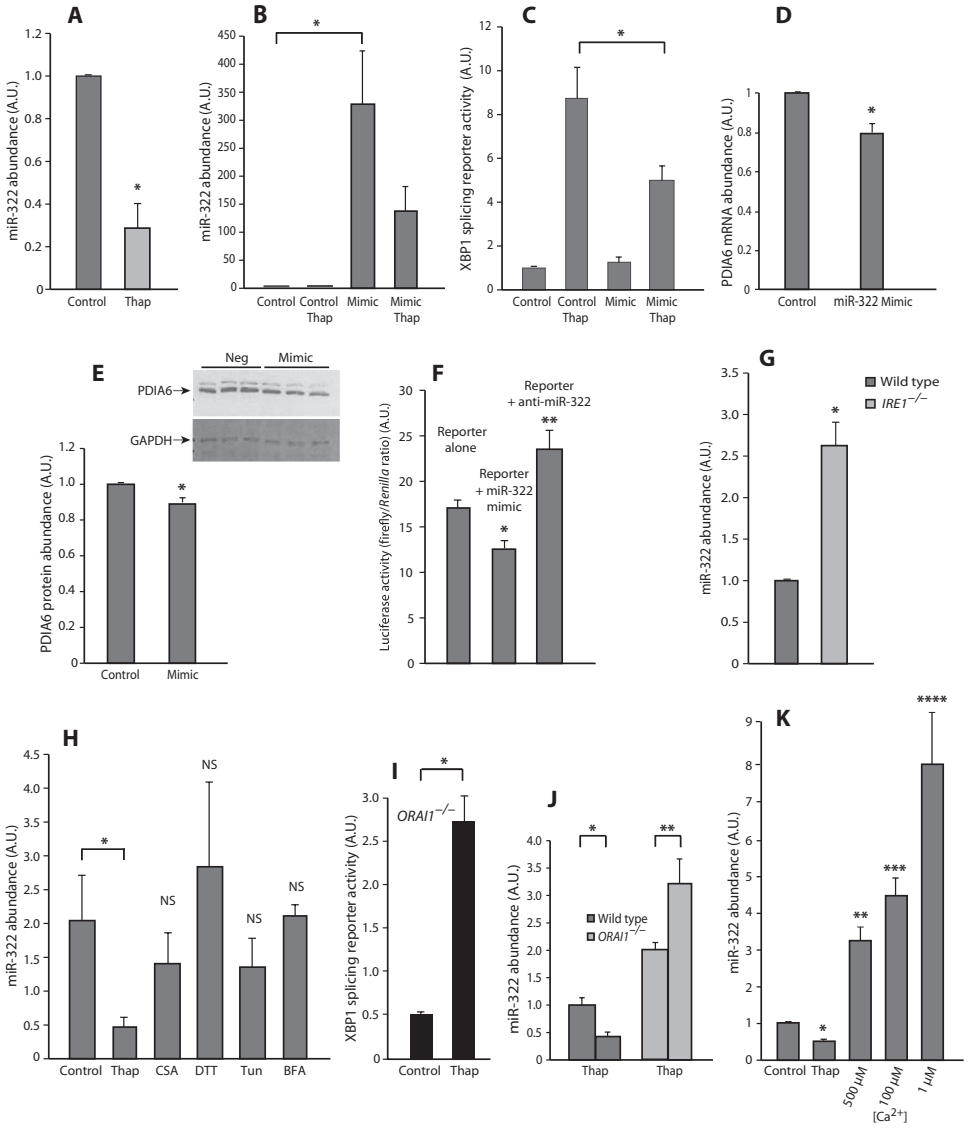

Fig. 3. miR-322 abundance is regulated by ER stress. (A) qPCR analysis of miR-322 abundance. *P = 0.0073. (B) qPCR analysis of miR-322 abundance in NIH-3T3 fibroblasts transfected with miR-322 mimic (Mimic) and treated with thapsigargin (Thap). *$P = 2.31 \times 10^{-6}$. Data are representative of more than three biological replicates. (C) NIH-3T3 fibroblasts were transfected with miR-322 mimic and XBP1 splicing reporter to monitor IRE1α activity. *P = 0.0383. (D) NIH-3T3 fibroblasts transfected with miR-322 mimic, followed by treatment with thapsigargin. PDIA6 mRNA abundance was assessed by qPCR. *P = 0.0002. (E) NIH-3T3 fibroblasts were transfected with miR-322 mimic, followed by treatment with thapsigargin. *P = 0.0366. Inset: Western blot representing three independent experiments was first probed with PDIA6 antibodies (top), stripped, and then reprobed with glyceraldehyde 3-phosphate dehydrogenase (GAPDH) antibodies (bottom). Neg, negative scrambled control siRNA. (F) PDIA6 3′UTR reporter activity in the presence of miR-322 mimic or inhibitor. *P = 0.0001 (mimic), **P = 0.029 (inhibitor). (G) miR-322 abundance in wild-type and *IRE1*$^{-/-}$ mouse embryonic fibroblasts. *P = 0.0045. Data are representative of more than three biological replicates. (H) NIH-3T3 fibroblasts were treated with thapsigargin, CSA, DTT, tunicamycin (Tun), or brefeldin A (BFA). *P = 0.0073. (I) XBP1 splicing in ORAI1-deficient cells. *ORAI1*$^{-/-}$ fibroblasts, *P = 0.0061. (J) miR-322 in *ORAI1*$^{-/-}$ fibroblasts. *P = 0.0061, **P = 0.0123. (K) miR-322 abundance in cells treated with thapsigargin or with different extracellular Ca^{2+} concentrations. *P = 0.0036; **P = 0.0006; ***P = 0.001; ****P = 0.0022. All data are representative of more than three biological replicates.

a plasma membrane Ca^{2+} channel that is responsible for SOCE (*12*). Depletion of ER Ca^{2+} stores with thapsigargin results in activation of ORAI1, Ca^{2+} entry, and a rapid increase in the cytosolic Ca^{2+} concentration (*12*). In the absence of ORAI1, Ca^{2+} depletion of ER stores with thapsigargin does not promote SOCE, and cytosolic Ca^{2+} remains at the resting concentration (*12*, *14*). In *ORAI1*$^{-/-}$ cells, thapsigargin-induced ER stress, as monitored by XBP1 mRNA splicing, was increased (Fig. 3I). In addition, these cells had increased miR-322 abundance as compared to the wild-type cells, and this was further increased with thapsigargin (Fig. 3J). These results indicated that thapsigargin-induced ER Ca^{2+} depletion at resting cytosolic Ca^{2+} concentrations in the absence of SOCE may have been ineffective in suppressing miR-322 abundance. An increase in miR-322 abundance in ORAI1-deficient cells pointed at a potential additional role of cytosolic Ca^{2+} in processing this miRNA. Next, we varied extracellular Ca^{2+} concentration in the absence of thapsigargin to reduce both ER stores and cytosolic Ca^{2+} concentrations. Lowering the extracellular Ca^{2+} concentration from 500 to 1 μM, a condition that reduces the cytosolic Ca^{2+} concentration but may also modify ER Ca^{2+} content, resulted in a concomitant increase in miR-322 abundance (Fig. 3K). Together, these data suggested that under conditions of ER stress and UPR activation due to disrupted ER Ca^{2+} homeostasis and activation of SOCE, miR-322 abundance was reduced. In contrast, reduction of cytosolic Ca^{2+} in the absence of Ca^{2+} store depletion and SOCE led to an increase in miR-322 abundance, although there is the possibility that ER Ca^{2+} was altered by these experimental conditions.

PDIA6 and miR-322 are regulated by ER stress in vivo

To establish the effect of PDIA6 on XBP1 splicing in vivo, we induced ER stress in mice and *Caenorhabditis elegans* and analyzed PDIA6 protein and mRNA abundance, miR-322 abundance, and PDIA6-dependent XBP1 splicing. In agreement with the in vitro analysis (Fig. 1C), PDIA6 abundance was significantly increased in the livers of mice injected with tunicamycin to induce ER stress (Fig. 4A). Full activation of XBP1 mRNA splicing and increases in the abundance of CHOP and BiP occur in this in vivo animal model (*37*). We also observed a concomitant reduction in miR-322 abundance in the livers of mice under induced ER stress (Fig. 4B), although miR-322 abundance

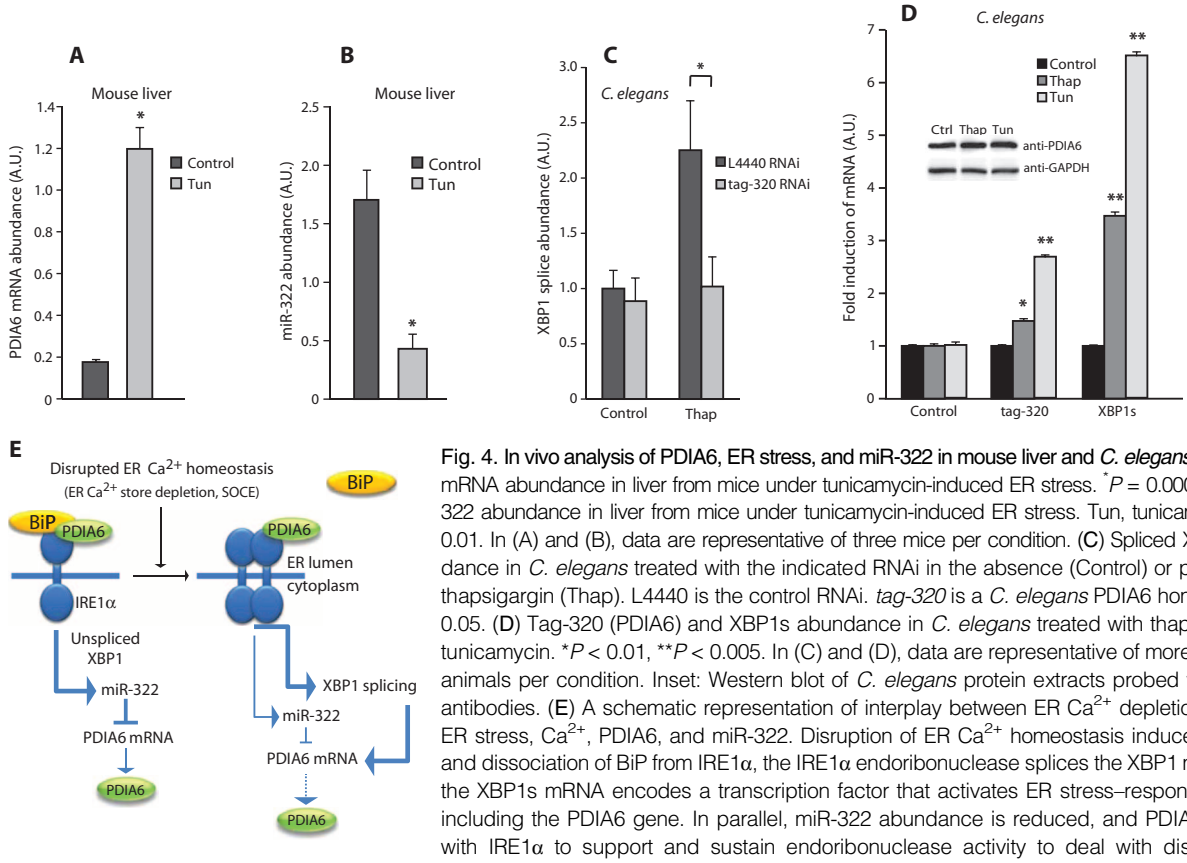

Fig. 4. In vivo analysis of PDIA6, ER stress, and miR-322 in mouse liver and *C. elegans*. (**A**) PDIA6 mRNA abundance in liver from mice under tunicamycin-induced ER stress. $^{*}P = 0.0001$. (**B**) miR-322 abundance in liver from mice under tunicamycin-induced ER stress. Tun, tunicamycin. $^{*}P = 0.01$. In (A) and (B), data are representative of three mice per condition. (**C**) Spliced XBP1 abundance in *C. elegans* treated with the indicated RNAi in the absence (Control) or presence of thapsigargin (Thap). L4440 is the control RNAi. *tag-320* is a *C. elegans* PDIA6 homolog. $^{*}P < 0.05$. (**D**) Tag-320 (PDIA6) and XBP1s abundance in *C. elegans* treated with thapsigargin or tunicamycin. $^{*}P < 0.01$, $^{**}P < 0.005$. In (C) and (D), data are representative of more than three animals per condition. Inset: Western blot of *C. elegans* protein extracts probed with PDIA6 antibodies. (**E**) A schematic representation of interplay between ER Ca^{2+} depletion–induced ER stress, Ca^{2+}, PDIA6, and miR-322. Disruption of ER Ca^{2+} homeostasis induces the UPR and dissociation of BiP from IRE1α, the IRE1α endoribonuclease splices the XBP1 mRNA, and the XBP1s mRNA encodes a transcription factor that activates ER stress–responsive genes including the PDIA6 gene. In parallel, miR-322 abundance is reduced, and PDIA6 interacts with IRE1α to support and sustain endoribonuclease activity to deal with disrupted ER homeostasis–induced ER stress. Dashed line indicates a modest effect.

was only somewhat reduced in tunicamycin-treated NIH-3T3 cells (Fig. 3H).

To test whether PDIA6 affected XBP1 mRNA splicing, we measured XBP1s transcript abundance in *C. elegans* treated with RNA interference (RNAi) against *tag-320*, the *C. elegans* homolog of PDIA6. Knockdown of *tag-320* reduced the thapsigargin-induced increase in XBP1s mRNA abundance (Fig. 4C). Furthermore, tag-320 abundance was increased at the mRNA level when worms were under ER stress induced by thapsigargin or tunicamycin (Fig. 4D). These results suggested that tag-320 was functionally required for XBP1 mRNA splicing, and that *tag-320* expression was also inducible in nematodes challenged with ER stress.

DISCUSSION

A critical function of the UPR is the recovery of normal functions of the cell by halting protein translation and activating signaling pathways that lead to increased production of molecular chaperones. The disruption of energy and/or nutrient balance is a fundamental cause of ER stress, and induces various corrective strategies. The ER stress coping responses help to reestablish ER and cellular proteostasis and ensure cell survival. Here, we focused on the identification of ER stress coping responses induced by alterations of ER Ca^{2+} homeostasis and, consequently, by changes in cellular Ca^{2+} homeostasis induced by the ER Ca^{2+} store depletion. We performed siRNA arrays and miRNA profiling arrays to search for ER coping components. Our findings identified two unexpected levels of UPR modulation and point at a potential regulatory network involving a specific miRNA and SOCE. We discovered that the ER oxidoreductase PDIA6 interacted with IRE1α. We demonstrated that PDIA6 was required for the maintenance of IRE1α activity as monitored by IRE1α phosphorylation, cluster formation, and downstream XBP1 mRNA splicing. ER Ca^{2+} depletion and activation of SOCE promoted changes in the abundance of different miRNAs, including miR-322, which targeted PDIA6 and regulated downstream IRE1α activity. We showed that in mouse and *C. elegans* animal models, PDIA6 and miR-322 abundance was modulated by ER stress and that PDIA6 influenced IRE1α signaling in *C. elegans*. It remains to be determined why ER stress induced by tunicamycin decreased miR-322 abundance in mice but not in cells. Silencing PDIA6 also induced global ER stress, suggesting that the protein has an important function in maintaining protein folding in the ER. Together, these findings suggested that interplay between ER Ca^{2+}, PDIA6, IRE1α, and miR-322 was part of a regulatory network activated by disrupted ER Ca^{2+} homeostasis that fine-tuned the UPR and probably the survival of cells undergoing ER stress. However, it will be necessary to perform additional, more precise manipulations to firmly establish the roles of Ca^{2+} in the cytosolic and ER compartments in the modulation of this regulatory network.

Figure 4E shows a schematic representation of the relationship between disrupted ER Ca^{2+} homeostasis, ER stress, IRE1α, PDIA6, and miR-322. BiP is a centrally located modulator and sensor of the ER stress response, and regulates all branches of the UPR. Under basal conditions, BiP binding to IRE1α desensitizes IRE1α to low amounts of stress and promotes its deactivation when favorable folding conditions are maintained

or restored to the ER. BiP forms complexes with PDIA6 [this work and (*21*, *22*)], and this study further showed that PDIA6 also bound to IRE1α. We propose a model in which, under basal conditions, IRE1α is not activated when complexed with BiP and low amounts of PDIA6, thus resulting in little splicing of XBP1 mRNA. The relatively high miR-322 abundance under these conditions results in low PDIA6 mRNA abundance. Disruption of ER Ca^{2+} homeostasis and activation of SOCE result in dissociation of BiP from IRE1α and rapid dimerization of IRE1α, leading to activation of its kinase and endoribonuclease activities. Under stress conditions, PDIA6 binding to IRE1α may sustain its long-term activity by stabilizing the dimeric or oligomeric state of the protein. This stabilization, combined with increased abundance of XBP1, increases the abundance of the PDIA6 protein and may allow the UPR to function robustly over time. Under the conditions of disrupted ER Ca^{2+} homeostasis, the interplay between Ca^{2+}, PDIA6, and miR-322 creates a reciprocal regulatory loop to promote sustained IRE1α activity to support corrective strategies to restore ER homeostasis.

The ER stress coping response is composed of distinct pathways controlled by common regulatory components (IRE1, PERK, ATF6, ATF4, and CHOP). BiP appears to function as a ligand for IRE1α, PERK, and ATF6. Here, we showed that other components of the ER luminal environment may regulate ER stress responses. The ability of PDIA6 to specifically affect IRE1α function supports the concept that the IRE1α, PERK, and ATF6 branches of ER stress are selectively modulated by additional mechanisms. This is in line with the identification of specific regulators of IRE1α that form a protein complex referred to as the UPRosome, of which PDIA6 may be a new component (*38*). It is likely that UPR pathways may function together as a single entity ("regulon") that would be controlled by the same regulatory system and would respond to ER stress in a coordinated fashion (*1*). Silencing PDIA6 during ER stress induced by Ca^{2+} store depletion had opposite effects on the IRE1α and ATF6 branches of ER stress responses, without affecting PERK signaling. Activation of ATF6 may compensate for the inhibition of IRE1α and would support a concept of ER stress–induced pathways (IRE1α, PERK, and ATF6), functioning in a coordinated fashion to respond to ER stress.

Disrupted ER Ca^{2+} homoeostasis decreased miR-322 abundance, thereby allowing increased PDIA6 abundance under conditions that stimulate ER stress. About 60% of the mRNAs of the cell are predicted to be regulated by miRNA function (*38*). At present, more than 1000 miRNAs have been identified in the human genome, with each miRNA targeting numerous mRNAs. In addition, one target mRNA may be regulated by multiple miRNAs (*39*). This work and other evidence point to a role for miRNAs during ER stress (*40*) and indicate that miRNAs regulate the cellular coping response under various stress conditions including ER stress. For example, miRNA profiles are changed during oxidative stress (*41*, *42*), nutrient deficiency (*43*, *44*), DNA damage (*45*–*47*), and oncogenic stress (*48*). Therefore, in response to stress, the cell may alter the gene expression program through regulation of miRNAs, which does not involve de novo synthesis of protein and therefore is a quicker response. Disruptions of specific miRNAs may not present a noticeable phenotype unless the system is stressed (*40*). For example, mice lacking miR-208 do not have an overt phenotype unless stressed with cardiac overload (*49*). As well, *Drosophila* lacking miR-7 show a breakdown in eye development when subjected to alternating temperatures (*50*), and inactivation of miR-8 in *Danio rerio* prevents responses to osmotic stress (*51*).

One way in which ER stress regulates miRNA abundance could be through direct regulation of miRNA expression by members of the ER stress pathway. ER stress–dependent activation of ATF6 decreases the abundance of miR-455 as a coping mechanism, contributing to the protective effects of ATF6 in the heart (*52*). Other coping mechanisms involve the transcription factors CHOP and XBP1, which regulate miR-708 and miR-346, respectively (*29*, *53*). The Dicer splicing machinery itself is activated by calpain and Ca^{2+} (*54*). Dicer is involved in processing small hairpin precursors (pre-miRs) into mature miRNAs that become associated with Argonaute to form RNA-induced silencing complexes (RISCs). Exposure of a neuronal cell line to increased extracellular Ca^{2+} results in the appearance of the active form of Dicer, as well as the full-length form of Argonaute, both cleaved by activated calpain, possibly leading to direct cleavage of pri-miRNAs (*55*). The endoribonuclease activity of IRE1α directly cleaves the pri-RNA cluster complex of miR-17 to antagonize classical Dicer processing of miR-17, thereby promoting apoptosis (*35*). IRE1α may regulate miR-322 in a similar manner as miR-17 because miR-322 has nucleotide sequences similar to the IRE1α endonuclease target sites in the IRE1α endoribonuclease substrates miR-17 and XBP1 mRNA. In support of this possibility, we showed that the IRE1α-deficient cells have significantly increased miR-322 abundance. This study suggests that the decreased abundance of miR-322 during disrupted ER Ca^{2+} homeostasis could rely on changes in the cytosolic Ca^{2+} concentration specifically provided by SOCE. ER Ca^{2+} depletion and activation of SOCE were at least partially necessary for the decreased abundance of miR-322 under ER stress conditions. We showed that miR-322 abundance was increased in ORAI1-deficient cells, which lack SOCE and have reduced cytosolic Ca^{2+} in the absence of SOCE. Together, these findings suggest that the disruption in ER Ca^{2+} homeostasis due to depletion of ER Ca^{2+}, activation of SOCE, and SOCE-independent changes in the cytosolic Ca^{2+} may differentially control the transcriptional regulation of this miRNA.

On the basis of the increasing relevance of the UPR for the development of several human diseases, including cancer, neurodegeneration, and diabetes (*1*), as well as advances in therapeutic strategies to target the UPR in diseases (*56*), our study provides potential points of manipulation of the UPR through the IRE1α, PDIA6, and miR-322 axis.

MATERIALS AND METHODS

Plasmids and site-specific mutagenesis

The pRL-IXFL XBP1 splicing reporter contained an internal *Renilla* control and the nucleotide sequence encoding XBP1 followed by firefly luciferase separated by an internal ribosomal entry site (IRES) initiation region (*13*). This reporter will only generate firefly luciferase activity if the XBP1 complementary DNA (cDNA) is spliced in-frame with the cassette encoding firefly luciferase. The Cignal Luciferase Reporter Assays were from Qiagen (cat. nos. CCS-9031L and CCS-2032L). Expression vector IRE1-NLD was constructed as described in (*23*) and used for site-specific mutagenesis. The following DNA primers were used for site-specific mutagenesis of IRE1-NLD: for C109A mutation, forward: 5′-GAATTGGTGCAGGCATCCCCAGCCCGAAGTTCAGATGGAATCC-3′ and reverse: 5′-GGATTCCATCTGAACTTCGGGCTGGGGATGCCTGCACCAATTC-3′; for C148A mutation, forward: 5′-GGCCTTTGCAGATAGTCTCGCCCCATCAACCTCTCTTCTG-3′ and reverse: 5′-CAGAAGAGAGGTTGATGGGGCGAGACTATCTGCAAAGGCC-3′; for C332A mutation, forward: 5′-GGGACAAGGGGGAGGCTGTGATCACGCCC-3′ and reverse: 5′-GGGCGTGATCACAGCCTCCCCCTTGTCCC-3′.

Cell culture, transfection, and siRNA library screen

NIH-3T3 mouse fibroblasts, ORAI1-deficient mouse fibroblasts, IRE1α-deficient mouse embryonic fibroblasts, and COS-1 cells were maintained under standard tissue culture conditions, including 5% CO_2 with high humidity. Tissue culture medium included 10% fetal bovine serum (FBS) in Dulbecco's modified Eagle's medium (DMEM) (both from Sigma). The siRNA library (Ambion) was pooled and aliquoted into 96-well full-skirt

PCR plates (Axygen) (*57*). Reverse transfection was performed, which involved preparation of a mixing plate containing the siRNA, plasmid DNA, Dharmafect Duo (GE), and Optimem (Life Technologies), followed by the addition of cells and plating into white 96-well plates (Corning) for 48 hours. Briefly, mixing plates were prepared containing 22 μl of 200 nM siRNA per well in a deep well format, followed by the addition of a mixture of 42 μl of Optimem (Invitrogen), 22 μl of XBP1 splicing reporter (20 μg/ml), 1.76 μl of Dharmafect Duo, and 352 μl of 1.2×10^5 cells/ml per well. The plates were mixed with four mixing cycles using the PerkinElmer robot, and then 100 μl was aliquoted into the wells of four white 96-well plates (four technical replicates). The plates were then incubated. Drug treatment consisted of removal of 50 μl of the medium, followed by the addition of 50 μl of 1 μM thapsigargin in DMEM with 10% FBS, bringing the final concentration of thapsigargin to 0.5 μM. Cells were incubated with thapsigargin for 24 hours, followed by removal of medium. Cell lysis was performed in a plate with 20 μl of Passive Lysis Buffer (Promega), followed by the luciferase assay, and analyzed with a PerkinElmer EnVision 2104 multilabel plate reader (PerkinElmer). Briefly, 100 μl of luciferase buffer [20 mM tricine (pH 7.2), 1.07 mM $MgCO_3$, 2.67 mM $MgSO_4$, 0.1 mM EDTA, 33.3 mM DTT, 270 μM coenzyme A, 470 μM luciferin, 530 μM ATP] was added to each well. Luciferase activity was monitored within 30 s from the addition of the luciferase buffer to minimize loss of signal.

The secondary screen involved computer-directed and robot-generated picking of statistically significant siRNA for 400 genes, including siRNA that either increased or decreased ER stress. siRNAs for each gene were randomly placed in 96-well full-skirt PCR plates (Axygen). These plates also included the water, negative, and positive control samples. A similar transfection was performed as above, using mixing plates to combine the ingredients for the transfection, except that volumes were calculated for technical triplicates, followed by 48 hours of incubation to allow silencing to occur. Drug application was performed in a similar manner as above, with harvesting after 24 hours using 20 μl of Passive Lysis Buffer according to the manufacturer's protocol. Dual luciferase assay analysis (Promega) was performed by adding 50 μl of LARII buffer that gives the firefly luciferase signal, followed by the addition of 50 μl of the Stop and Glo buffer to generate the *Renilla* signal according to the manufacturer's protocol (*58*). Cell viability assays were carried out three times in biological triplicate in a 96-well format using the pooled siRNA for each gene selected as described above, including a negative siRNA control and a nonsilencing control. Results are presented as normalized to the internal *Renilla* expression and untreated negative scrambled control siRNA set at 1. Cell growth was analyzed using the MTS Cell Proliferation Assay (Promega) according to the manufacturer's protocol. Briefly, the tetrazolium compound MTS [3-(4,5-dimethylthiazol-2-yl)-5-(3-carboxymethoxyphenyl)-2-(4-sulfophenyl)-2*H*-tetrazolium] is biologically reduced by dehydrogenase enzymes found in metabolically active cells into a formazan product that is soluble. The amount of formazan measured at an absorbance of 490 nm is directly proportional to the number of living cells.

To validate our screening results, Dharmacon siGENOME Smartpools were used to silence the selected genes. Manual large format siRNA transfections were performed more than three times in technical triplicate using 48- or 24-well plates with siRNA for each selected gene. Conditions were maintained according to the primary library screen and scaled up two- or fourfold to account for 48- or 24-well plates, respectively. Results were obtained using the dual luciferase assay analysis according to the manufacturer's protocol. The following are the nucleotide sequences of the siRNAs used in this study: PDIA6 (Thermo Scientific, siGENOME Smartpool and set of 4 upgrade), 5′-UCGAUUUGUUCUCUGAUAA-3′ (siRNA #1), 5′-GCCUGUGGCUUGUAGAAUU-3′ (siRNA #2), 5′-GAUAAUCAACGAAGACAUA-3′ (siRNA #3), and 5′-GGUGAUAGUUCAAGUAAGA-3′ (siRNA #4); BiP (Silencer, Ambion), 5′-GGACAUCAAGUUCUUGCCATT-3′, 5′-GGUGGUUGAAAAGAAAACUTT-3′, and 5′-GGUUACCCAUGCAGUUGUUTT-3′; IRE1α (Silencer, Ambion), 5′-CCUUGUUGUUUGUCUCGACTT-3′, 5′-GGCCUGACGAAACUUCCCUTT-3′, and 5′-GCAAGCUGAACUACUUGAGTT-3′; and negative control siRNA (Ambion, cat. no. AM4635).

Statistical analysis of primary and secondary siRNA library screen

Before statistical analyses of the primary and secondary library screens, values on the plate were shifted by the average water readout. Then for each siRNA, the average was computed from four technical replicates; the value of the replicate that was furthest from the average was removed as an outlier. The average was then computed using only the values of the three remaining replicates and was used as a representative value. Next, for each treatment, all representative siRNA values were converted into *P* values, using the SN package (*59*) for R platform to fit the skewed normal distribution. Finally, for each treatment, the 400 most extreme *P* values (containing a mix of the lowest and the highest values) were selected and used in the secondary screen with the dual luciferase reporter assay.

The results from the secondary screen were normalized as previously described (*60*). Because each plate contained a different set of siRNAs, the 16 wells that had the same content along all plates were used as a normalization baseline. The firefly/*Renilla* (F/R) fold changes for the above-mentioned 16 wells across all plates were computed, and these values were used to normalize all plates using the first plate as reference. After normalization, the average from two replicates was used as the representative F/R readout for an siRNA. Similar to the first round, the CDF (cumulative distribution function) values were generated using skewed normal distributions, which were fitted to the data.

Protein purification, pull-down, and BIACore analyses

PDIA6 was isolated from mouse liver microsomal fraction. In brief, livers were homogenized using a buffer containing 37.5 mM tris maleate (pH 6.4), 150 mM NaCl, 5 mM $MgCl_2$, and 250 mM sucrose. The resulting mixture was centrifuged at 10,000*g* for 30 min at 4°C. The supernatant was further centrifuged at 100,000*g* for 90 min at 4°C. The pellet containing microsomes was washed with 10 mM tris (pH 7.4) and resuspended in 10 mM tris (pH 7.4) and 20% glycerol and stored at −80°C. The microsomes were permeabilized with a buffer containing 1% Triton X-100, 25 mM KCl, 5 mM $MgCl_2$, and 50 mM tris (pH 7.5); incubated on ice for 30 min; and centrifuged at 100,000*g* for 90 min at 4°C. The supernatant was subjected to 50% ammonium sulfate precipitation followed by centrifugation at 10,000*g* for 15 min. Ammonium sulfate was added to the supernatant to 93% saturation, followed by 30-min incubation and centrifugation at 10,000*g* for 15 min. The 93% ammonium sulfate cut pellet containing PDIA6 was dialyzed against a buffer containing 20 mM Hepes (pH 7.5), 25 mM KCl, and 5 mM $MgCl_2$. The dialyzed protein was then loaded onto a 5-ml concanavalin A affinity column (to remove glycosylated proteins). The flow through containing PDIA6 was heat-treated at 54°C for 15 min followed by centrifugation at 30,000*g* for 40 min to remove non–heat-stable proteins (PDIA6 is heat-stable). The supernatant was then applied in the presence of Ca^{2+} to a phenyl-Sepharose column (many Ca^{2+} binding proteins in the ER bind to phenyl-Sepharose in the presence of Ca^{2+}). The fractions containing PDIA6 were collected, and proteins were separated by Sephadex G-50 chromatography. PDIA6 co-eluted with BiP. BiP was separated from PDIA6 by ATP-agarose chromatography in a buffer containing 20 mM Hepes (pH 7.5), 135 mM KCl, 20 mM $MgCl_2$, and 1 mM DTT. PDIA6 was eluted in the void volume, whereas BiP, an ATP binding protein, was retained on the column.

BiP was eluted from the ATP-agarose with 10 mM ATP. Samples purified using this protocol resulted in more than 95% pure BiP and about 90% pure PDIA6.

IRE1α ER luminal domain (IRE1-NLD) or IRE1-NLD cysteine triple mutant were expressed in COS-1 cells and purified by Ni-NTA-agarose (*23*). COS-1 cells were transfected with IRE1-NLD expression vector, harvested, and lysed in a buffer containing 25 mM tris-Cl (pH 8.0), 150 mM NaCl, and 1% NP-40. Cell lysates were centrifuged at 20,000*g* for 15 min, and cell extracts were used for protein purification. Ni-NTA-agarose chromatography was carried out using a buffer containing 50 mM tris-Cl (pH 8.0), 500 mM NaCl, and 5 mM imidazole. The IRE1-NLD protein was eluted with 100 mM imidazole and concentrated.

For pull-down experiments, COS-1 cells were transfected with pED-IRE1-NLD-His6 expression vector. Cells were further treated with 0.5 μM thapsigargin for an additional 24 hours. Formaldehyde was added directly to the culture to 1% final concentration, and the culture was incubated for 20 min. Cross-linking was quenched by the addition of 0.5 M glycine. Cells were harvested by washing with cold tris-buffered saline followed by scraping into cold radioimmunoprecipitation assay (RIPA) buffer [50 mM tris (pH 7.2), 150 mM NaCl, 0.1% SDS, 0.5% sodium deoxycholate, 1% NP-40, protease inhibitors]. The lysate was incubated on ice for 30 min, followed by centrifugation and overnight incubation at 4°C with 100 μl of 10% slurry of Ni-NTA-agarose beads (Qiagen). The beads were centrifuged briefly to pellet, and washed three times with 1.5 ml of RIPA buffer, three times with 1.5 ml of RIPA buffer with 20 mM imidazole, and two times with 1.5 ml of buffer containing 10 mM tris-HCl (pH 8.0) and 1 mM EDTA. The beads were pelleted, boiled in SDS–polyacrylamide gel electrophoresis (SDS-PAGE) sample buffer, separated on SDS-PAGE (10% acrylamide), and analyzed by Western blot with antibodies against IRE1α, PDIA6, and tubulin.

For BIACore analysis, the carboxymethylated dextran (CMD) surface of a CM5 chip was activated using *N*-hydroxysuccinimide (NHS)/1-ethyl-3(3-dimethylaminopropyl)-carbodiimide hydrochloride (EDC). IRE1-NLD or IRE1-NLD cysteine triple mutants (C109,148,332A-IRE1-NLD) were captured at a flow rate of 5 μl/min to a total of ~2000 response units. Uncoupled amine reactive sites on the CMD surface were then blocked by an injection of ethanolamine. The CM5 chip was normalized and prepared for kinetic analysis. PDIA6 in a buffer containing 10 mM Hepes (pH 7.4), 150 mM NaCl, and 0.005% P20 at concentrations from 0 to 5000 nM was passed over the sensor surface at a flow rate of 30 μl/min. The BIACore analysis was also performed in a buffer containing 2 mM $CaCl_2$ or 2 mM EGTA. Kinetic analysis was performed in biological triplicate. All experiments were conducted on a BIACore 3000 or BIACore T200 instrument (GE). For surface plasmon resonance analysis with cysteine blocking, 200 μM NEM was injected for 60 s at a flow rate of 30 μl/min over the captured IRE1-NLD. Addition of NEM alone did not result in a binding response. PDIA6 was then injected at a flow rate of 30 μl/min for 30 s over the captured IRE1-NLD. The cysteine blocking experiment was performed three times.

MicroScale Thermophoresis

MST assays were carried out with a Monolith NT.115 instrument (Nano Temper) (*61*). To evaluate PDIA6 binding to IRE1-NLD, an increasing concentration of purified IRE1-NLD (0 to 1 μM) was used against fluorescein isothiocyanate–labeled PDIA6. Experiments were carried out in a buffer containing 10 mM Hepes (pH 7.4), 100 mM NaCl. Data evaluation was performed with the Monolith software.

XBP1 splicing and RIDD analysis

The quantitative analysis of spliced and total XBP1 transcripts in mammalian cells protocol was used to identify mouse XBP1 specific splicing with a pair of real-time PCR primers designed for quantification of mouse *XBP1* mRNA splicing (*62*). The forward primer sequence was 5′-GAGTCCGCAGCAGGTG-3′ (mouse), and the reverse primer sequence was 5′-GTGTCAGAGTCCATGGGA-3′ (mouse). Pairs of real-time PCR primers were also designed for quantification of mouse total *XBP1* mRNA. The forward primer was 5′-AAGAACACGCTTGGGAATGG-3′ (mouse), and the reverse primer was 5′-ACTCCCCTTGGCCTCCAC-3′ (mouse). These pairs of real-time PCR primers amplified both the unspliced and spliced forms of *XBP1* mRNA transcripts. SYBR Green PCR Master Mix (Bio-Rad 170-8880S) was used to set up the quantitative real-time PCR; the reaction (20 μl) contained 500 nM forward and reverse primers, 10 to 100 ng of cDNA templates made from murine total RNA, and 1× SYBR Green Supermix [50 mM KCl, 20 mM tris-HCl (pH 8.4), 0.2 mM of each deoxynucleotide triphosphate, iTaq DNA polymerase (25 U/ml), 3 mM $MgCl_2$, SYBR Green 1, 10 nM fluorescein, and stabilizers]. The thermal cycling parameters were step 1: 95°C for 10 min; step 2: 95°C for 20 s, 58°C 15 s, 72°C for 15 s. Step 2 was repeated for 40 cycles. The specificity of the amplification product from each primer pair was confirmed by melting curve analysis of the PCR product. Quantification was performed by expressing the threshold for each gene as a cycle number (Ct) and normalizing it to a housekeeping gene such as GAPDH, actin, or β-tubulin using the equation $1/2^{[Ct(gene) - Ct(gapdh)]}$ and subsequently to the untreated negative siRNA control.

To measure the mRNA abundance of unspliced XBP1 and XBP1s, reverse transcription PCR (RT-PCR) was performed using total RNA isolated by TRIzol (Invitrogen) and the RNeasy kit (Qiagen) followed by PCR using specific primers. The PCR product was purified and then cleaved with Pst I to generate two smaller fragments. Only the unspliced XBP1 can be cleaved by Pst I, whereas XBP1s has the Pst I site removed by the splicing event. Samples were separated on a 2% agarose gel, with densitometry performed on the digested and undigested fragments, to determine the amount of splicing occurring in endogenous XBP1. Mouse sequence-specific primers for XBP1 splicing were forward: 5′-CCTTGTGGTTGAGAACCAGG-3′ and reverse: 5′-CTAGAGGCTTGGTGTATAC-3′.

For measuring RIDD activity, total RNA was prepared from cells using TRIzol (Invitrogen), and cDNA was synthesized with SuperScript III (Invitrogen) using random primers p(dN)6 (Roche). Quantitative real-time PCR reactions were done using Brilliant II SYBR Green qPCR Master Mix (Agilent Technologies). The relative amounts of mRNAs were calculated from the values of comparative threshold cycle by using *rpl19* as control. The following primers were used for human cells: *scara*, 5′-GAGCCGTGTGTAGTTCTGCC-3′ and 5′-TCACCCAGGAGTGCTACGAT-3′; *rpl19*, 5′-TCAGGTACAGGCTGTGATACA-3′ and 5′-GGGCATAGGTAAGCGGAAGG-3′; and *col6*, 5′-GATAGCGCAGTCGGTGTAGG-3′ and 5′-ACAGTGACGAGGTGGAGATCA-3′.

Western blot analysis, immunoprecipitation, and Ca^{2+} measurements

Large format siRNA transfection was performed a minimum of three times in duplicate using 24-well plates with the siRNA for the selected genes. Cells were harvested at day 3 after siRNA transfection using RIPA lysis buffer [50 mM tris (pH 7.5), 150 mM NaCl, 1 mM EDTA, 1 mM EGTA, 1% Triton X-100, 0.1% SDS, 0.5% sodium deoxycholate] containing protease inhibitors (*63*). Protein assays were performed using the Bio-Rad protein assay, and 20 μg of protein was loaded in each lane on an SDS-PAGE gel and, after electrophoresis, transferred onto nitrocellulose. Antibodies used were rabbit anti-PDIA6 (Abcam, ab11432), rabbit anti-BiP (Abcam, ab21685), rabbit anti-IRE1α (Abcam, ab37073), goat anti-calreticulin, rabbit anti-GAPDH (Abcam, ab9483), and rabbit anti-tubulin (Abcam, ab6046). Antibodies were used at a dilution of 1:500, except

anti-GAPDH (1:300), anti-calreticulin (1:300), and anti-tubulin (1:2000). Western blot images were scanned, and densitometry was performed using ImageJ and plotted in Excel.

Immunoprecipitations were performed with lysates of NIH-3T3 fibroblasts, except when it was necessary to detect IRE1α in the immunoprecipitates. In this case, it was necessary to perform immunoprecipitations with lysates of COS-1 cells expressing IRE1α-NLD. Both NIH-3T3 fibroblasts and transfected COS-1 cells were treated with 0.5 μM thapsigargin for 24 hours. Proteins were cross-linked using 4% formaldehyde for 12 min, followed by 15 min of quenching with 100 mM glycine in phosphate-buffered saline (PBS) and extensive washing with PBS. Lysates were harvested with RIPA buffer. Protein assays were performed, and the lysate was diluted to 1 mg/ml. Lysates were precleared with 60 μl of a 10% slurry of protein A/G–Sepharose beads (Roche). Two microliters of antibody (control immunoglobulin G, rabbit anti-PDIA6, rabbit anti-IRE1α, or rabbit anti-BiP) was added, and lysates were incubated overnight at 4°C with rotation. One hundred microliters of a 10% slurry of protein A/G–Sepharose was added, and lysates were incubated for 4 hours with rotation at 4°C. Beads were pelleted and washed with RIPA buffer five times. Pellets were resuspended in 60 μl of sample buffer and loaded on a SDS-PAGE gel followed by protein transfer. Western blot analysis was carried out with specific antibodies as indicated above.

Ca^{2+} measurements were performed as previously described (*14*, *64*). Fura-2 acetomethylester fluorescence was monitored in a scanning spectrofluorometer (Photon Technology International). ER Ca^{2+} release was induced by 200 nM thapsigargin or 100 μM ATP, with SOCE induced by the addition of 4 mM $CaCl_2$. To chelate extracellular Ca^{2+}, EGTA was added to DMEM at concentrations from 1 to 4 mM. The EGTA calculator MaxChelator (maxchelator.stanford.edu) was used to determine free Ca^{2+} concentration in growth medium. The initial (prechelator) $[Ca^{2+}]_{total}$ in DMEM (Invitrogen) was assumed to be 1.8 mM. FBS contains about 3.7 mM Ca^{2+}. Addition of 50 ml of FBS added 0.37 mM Ca^{2+} to 500 ml of DMEM, giving a final concentration of 2.17 mM Ca^{2+} in complete medium. EGTA was added at various concentrations to reach three final Ca^{2+} concentrations: 1.67 mM EGTA for 500 μM Ca^{2+}, 2.08 mM EGTA for 100 μM Ca^{2+}, and 3.25 mM EGTA for 1 μM Ca^{2+}. Cells were grown for 24 hours in regular medium, followed by washing with PBS and addition of varying amounts of Ca^{2+} concentrations for 24 hours.

RT-PCR and qPCR for mRNA and miRNA

To monitor mRNA abundance, cells were harvested at day 3 after large format siRNA transfection using TRIzol (Invitrogen). RNA was isolated using the RNeasy kit (Qiagen), and total RNA (200 ng) was subsequently used in RT-PCR to generate cDNA for each sample. To monitor mRNA abundance, the cDNA was diluted 10-fold, with 2 μl of cDNA used in subsequent PCR reactions with primers targeting controls or selected genes. qPCR was performed using the LightCycler rapid thermal cycler system (Corbett Research) according to the manufacturer's instructions. Reactions were performed in a 20-μl volume with 0.5 μM primers. Other reagents including nucleotides, Taq DNA polymerase, and buffer were used as provided in the SYBR Green Master Mix (Bio-Rad). The amplification protocol included 10 min of 95°C denaturation and 40 cycles with 95°C denaturation for 15 s, 58°C annealing for 15 s, and 72°C extension for 15 s. Detection of the fluorescent product occurred at the end of the 72°C extension period. The specificity of the amplification product from each primer pair was confirmed by a melting curve analysis of the PCR product. Quantification was performed as described above. The following nucleotide primers were used for RT-PCR and qPCR analyses: for PDIA6, forward: 5′-TCTGGTGAGCTGCACCTTCTTTCT-3′, reverse: 5′-AGCCGTTGCTGCTTTCTTCCATTC-3′; for GAPDH, forward: 5′-TTCACCACCATGGAGAAGGC-3′, reverse: 5′-GGCATGGACTGTGGTCATGA-3′; for BiP, forward: 5′-AAGCTCAAAGAGCGCATTGACACC-3′, reverse: 5′-AGTCTTCAATGTCCGCATCCTGGT-3′; for PDIA7, forward: 5′-AAATGCAGGGTGCTGTTACC-3′, reverse: 5′-AAGCCCTTCAATGGTGTGTTC-3′; for IRE1α, forward: 5′-TATGCCTCTCCCTCAATGGTGCAT-3′, reverse: 5′-TCAAACTTGAGGTCTGTGCTGGGA-3′; and for calreticulin, forward: 5′-AAGACTGGGATGAACGAGCCAAGA-3′, reverse: 5′-AATTTGACGTGGTTTCCACTCGCC-3′.

IRE1α cluster quantification and phosphorylation

T-REx293 IRE1-3F6HGFP cells (*24*) were transiently transfected with pcDNA3.1-PDIA6-V5 or pcDNA3.1 as control. Twenty-four hours after transfection, cells were split and reseeded on 25-mm-diameter coverslips in DMEM with 5% FBS and treated with doxycycline (5 μg/ml) for 24 hours to induce IRE1α-GFP expression, followed by the addition of 1 μM thapsigargin. Cells were fixed in 4% paraformaldehyde for 6 hours, followed by incubation with a blocking solution [0.25% bovine serum albumin (BSA), 10% horse serum in PBS] for 10 min. Cells were permeabilized with 0.5% NP-40 in 0.25% BSA, 10% horse serum in PBS for 10 min at room temperature. Samples were incubated sequentially with primary antibodies (mouse anti-V5, 1:500 dilution, Invitrogen) and secondary antibody (goat anti-mouse Alexa Fluor 594, Life Technologies) for 60 min at room temperature. Nuclei were stained with 4′,6-diamidino-2-phenylindole. Images were acquired using an Olympus FluoView FV1000 confocal laser-scanning microscope. Image stacks were captured using a 63×/1.4 objective with constant parameters for all conditions of each type of experiment, guaranteeing that the image was not saturated and that image background was slightly above zero. Twenty different fields were analyzed with a total of 150 to 200 cells per group in three independent experiments. The numbers of IRE1α clusters and cluster size were quantified using ImageJ for PDIA6-V5 positive and negative cells.

A Phostag assay was performed to monitor IRE1α phosphorylation (*37*). HEK293T cells were transiently transfected with PMSCV-IRE1α-HA and pcDNA3.1 or PMSCV-IRE1-HA and pcDNA3.1-PDIA6-V5 for 48 hours. Cells were treated with 50 nM thapsigargin for the indicated time points, and total cell extracts were analyzed by Western blot. Phostag assay was performed using 50 mg of total protein loaded in 8% SDS-PAGE minigel containing 25 mM of Phostag in the presence of 25 mM $MnCl_2$. The following antibodies and dilutions were used: anti-HA (1:1000, Covance), anti-V5 (1:10,000, Sigma), and anti–heat shock protein 90 (1:5000, Santa Cruz Biotechnology).

In vivo ER stress analysis

Wild-type mice were given a single intraperitoneal injection (50 ng/g body weight) of a suspension (0.05 mg/ml) of tunicamycin in 150 mM dextrose (*65*). After 16 hours, mice were euthanized and liver extracts were prepared for immunoblot or Q–PCR analyses. All animal experiments were performed according to procedures approved by the Animal Use Committee of the Faculty of Medicine of the University of Chile.

The wild-type N2 *C. elegans* strain (Bristol) was obtained from the *Caenorhabditis* Genetics Center at the University of Minnesota. Worm breeding and handling were conducted following standard methods as described previously (*66*). For RNAi experiments, synchronized first larval stage (L1) worms were placed on Nematode Growth Medium agar medium, which contained ampicillin (100 μg/ml) and 1 mM isopropyl-thio-β-D-galactoside and was seeded with an overnight culture of bacteria containing each RNAi clone (http://www.geneservice.co.uk). The worms were used for the analysis 3 days after RNAi application. The worms were treated with thapsigargin (3 μg/ml) for 5 hours. Total mRNA was extracted

from worms using the RNeasy Plus Mini Kit (Qiagen), cDNA was synthesized using the Prime Script RT reagent kit (TaKaRa), and the quantitative RT-PCR analysis was performed using the KAPA SYBR FAST qPCR kit (KAPA Biosystems) and the Thermal Cycler Dice Real Time System (TaKaRa) according to the manufacturers' protocols.

For analysis of PDIA6 expression in *C. elegans,* the worms were cultured in the RNAi-treated plates containing thapsigargin (3 μg/ml) or tunicamycin (5 μg/ml) for 5 hours. RNA was isolated for qPCR analysis, and worm extracts were used for Western blot analysis with antibodies against PDIA6 (Abcam, ab11432) and GAPDH (Abcam, clone 8C2). The following pairs of real-time PCR primers were used for quantification of *C. elegans* genes: for XBP1s, forward: 5′-TGCCTTTGAATCAGCAGTGG-3′ and reverse: 5′-ACCGTCTGCTCCTTCCTCAATG-3′; for PDI-1, forward: 5′-GAAAGCCAACGAAATACACCG-3′ and reverse: 5′-ACAACTCTGGTCTTTCCCTTC-3′; for PDI-2, forward: 5′-AGAGATCAAGTCGCACAACC-3′ and reverse: 5′-CGGTGTTGATGTAGACGAAGAG-3′; for PDI-3, forward: 5′-GTTGACAATCTCCAGCAATTCG-3′ and reverse: 5′-AACGTCTCTTGTTCATCTGG-3′; for tag-320, forward: 5′-CCCAACCATCAAGTATTTCGC-3′ and reverse: 5′-GCATGTTTTCTTGAGCACGAG-3′.

Deep sequencing analysis and selection of miRNA

Deep sequencing was performed by PlantBiosis (University of Lethbridge). NIH-3T3 fibroblasts were treated with 0.5 μM thapsigargin for 24 hours and harvested with TRIzol (Invitrogen). RNA was isolated using the RNeasy kit (Qiagen), and total RNA was used for deep sequencing. Statistical analysis was performed on the raw data. Short reads generated using Illumina GAIIx were cleaned up using the FastQC program (http://www.bioinformatics.bbsrc.ac.uk/projects/fastqc), continuous poly-A/T/C/G were removed, and adapters were trimmed at the 3′ end using the Btrim program (*67*). Sequences between 18 and 29 nucleotides in length were retained. The leading N base was trimmed at the 5′ end. The remaining short RNAs were filtered to find both known and putative (novel) miRNAs. Reads that did not match the National Center for Biotechnology Information (NCBI) mouse genome (using build 37.2 from http://www.ncbi.nlm.nih.gov/projects/genome/guide/mouse/) were discarded. Sequence alignment was performed using the Bowtie program (*68*) assuming perfect match. Reads that matched repetitive DNAs from Repbase (*69*) (uploaded from http://www.girinst.org/server/RepBase/) and noncoding RNAs, including transfer RNAs, ribosomal RNAs, small nuclear RNAs, and small nucleolar RNAs, from Rfam (*70*) (using build 10.0 from http://rfam.janelia.org/) were removed. Known miRNAs were tagged using release 17 of miRBase (*71*) and set aside. The remaining short RNAs were processed to find putative miRNAs. First, they were aligned to (i) mRNAs using RefSeq database (*72*) (the matching reads were tagged as mRNA-matching); and (ii) expressed sequence tags (ESTs) using dbEST (*73*) (the matching sequences were tagged as EST-matching). Two putative miRNA precursor sequences of the mRNA-matching, EST-matching, and the remaining short reads (one with 10 nucleotides upstream and 70 nucleotides downstream, assuming that miRNA is at the 5′ arm of the RNA hairpin, and the other with 70 nucleotides upstream and 10 nucleotides downstream, assuming that miRNA is at the 3′ arm) were processed by the MIREAP program (http://sourceforge.net/projects/mireap/) to select those that have hairpin structure. The hairpin-like reads were folded using RNAfold (*74*) to select those with a minimum free energy below −25 kcal/mol. Finally, the remaining short RNAs were clustered to group similar reads. Both miRNAs and miRNAs* were considered. Each cluster represents one putative miRNA, and its sequence was set to be the most frequent or abundant sequence in a given cluster. The abundance for each putative miRNA was calculated as a sum of abundance of all (similar) reads in this cluster.

Annotation of differentially expressed miRNAs

All known miRNAs and miRNAs*, which were annotated using miRBase, and putative miRNA and miRNAs* were combined together, and those with abundance (counts) below 5 were removed. Bioconductor package edgeR (*75*) was applied to determine whether a given miRNA was differentially expressed between the wild-type and knockout groups. The miRNAs were sorted by the adjusted *P* values, which were computed using trimmed mean of *M* values (TMM) normalization and tagwise dispersion. All miRNAs with adjusted $P > 0.5$ were annotated with their (putative) target genes and considered for experimental validation. The experimentally validated targets were collected using miRecords database (*76*). Because the number of experimental annotations was relatively low, we used three target predictors (*77*): TargetScan (*30*, *31*), DIANAmicroT (*32*), and RepTar (*33*). Targets that were associated with multiple annotations were considered to be more reliable. Statistically significant miRNAs were submitted to IPA (IngenuitySystems, http://www.ingenuity.com), generating a network of bioactive systems affected by these miRNAs.

miR-322 expression, treatment with mimic, and PDIA6 3′UTR reporter analysis

The miR-322 sequence specific mimic and inhibitor (Qiagen) were used at a final concentration of 20 nM. To measure the amount of miRNA present in samples, the samples were isolated with TRIzol (Invitrogen) and subjected to RNA purification using the RNeasy kit (Qiagen). To monitor the miRNA, a specific miRNA RT-PCR to generate cDNA was performed using the miRCURY LNA Universal RT miRNA PCR kit (Exiqon). This RT-PCR generates cDNA that corresponds to miRNA and contains a particular motif that can be recognized by specific primers for miRNA analysis (Exiqon). The cDNA was diluted 20-fold, and miRNA-specific primers were used in the subsequent qPCR. The qPCR was prepared as follows: 4 μl of cDNA, 2 μl of PCR primer mix (prepared by diluting forward and reverse primers 1:1), 4 μl of water, and 10 μl of SYBR Green Master Mix (Bio-Rad). The amplification protocol included 10 min of 95°C denaturation; 40 cycles with 95°C denaturation for 15 s, 58°C annealing for 15 s, and 72°C extension for 15 s. Detection of the fluorescent product occurred at the end of the 72°C extension period. The specificity of the amplification product from each primer pair was confirmed by a melting curve analysis of the PCR product. Quantification was performed as described above, except that 5S ribosomal RNA was used as the housekeeping control (Exiqon, cat. no. 203906). The mmu-miR-322 PCR Primer Set (Exiqon, cat. no. 205182) and mmu-miR-322 mimic (Qiagen, cat. no. MSY0000548) and inhibitor (Qiagen, cat. no. MIN0000548) were based on 5′-CAGCAGCAAUUCAUGUUUUGGA-3′. Results were normalized to the 5S control with untreated control set at 1.

For PDIA6 3′UTR reporter analysis, 3T3 fibroblasts were reverse-transfected with PDIA6 3′UTR Reporter (OriGene) vector (pMirTarget) with either miR-322 mimic or anti–miR-322 (Qiagen) to monitor miR-322 activity toward PDIA6 3′UTR. Luciferase activity was monitored using the dual luciferase activity assay (Promega).

Statistical analysis

As suggested in (*78*), if the measurements were normal, as evaluated with the Anderson-Darling test at 0.05 significance (*79*), then we used the *t* test; otherwise, we used the nonparametric Wilcoxon rank sum test (*80*). A difference was determined to be statistically significant if $P < 0.05$.

SUPPLEMENTARY MATERIALS

www.sciencesignaling.org/cgi/content/full/7/329/ra54/DC1
Fig. S1. The XBP1 splicing reporter system.
Fig. S2. A genome-wide siRNA screen.

Fig. S3. Silencing of the PDIA6 gene.
Fig. S4. Phosphorylation of eIF2α in PDIA6-silenced cells.
Fig. S5. PDIA6 mRNA abundance under ER stress conditions.
Fig. S6. PDIA6 interacts with the luminal domain of IRE1.
Fig. S7. PDIA6 silencing and IRE1α RIDD activity.
Fig. S8. Selected miRNAs identified by deep sequencing analysis.
Fig. S9. Schematic representation of multiple target prediction analysis.

REFERENCES AND NOTES

1. J. Groenendyk, L. B. Agellon, M. Michalak, Coping with endoplasmic reticulum stress in the cardiovascular system. *Annu. Rev. Physiol.* **75**, 49–67 (2013).
2. P. Walter, D. Ron, The unfolded protein response: From stress pathway to homeostatic regulation. *Science* **334**, 1081–1086 (2011).
3. S. Wang, R. J. Kaufman, The impact of the unfolded protein response on human disease. *J. Cell Biol.* **197**, 857–867 (2012).
4. Y. Kimata, K. Kohno, Endoplasmic reticulum stress-sensing mechanisms in yeast and mammalian cells. *Curr. Opin. Cell Biol.* **23**, 135–142 (2011).
5. H. Kraskiewicz, U. FitzGerald, InterfERing with endoplasmic reticulum stress. *Trends Pharmacol. Sci.* **33**, 53–63 (2012).
6. C. Hetz, The unfolded protein response: Controlling cell fate decisions under ER stress and beyond. *Nat. Rev. Mol. Cell Biol.* **13**, 89–102 (2012).
7. M. Calfon, H. Zeng, F. Urano, J. H. Till, S. R. Hubbard, H. P. Harding, S. G. Clark, D. Ron, IRE1 couples endoplasmic reticulum load to secretory capacity by processing the *XBP-1* mRNA. *Nature* **415**, 92–96 (2002).
8. K. Yamamoto, H. Yoshida, K. Kokame, R. J. Kaufman, K. Mori, Differential contributions of ATF6 and XBP1 to the activation of endoplasmic reticulum stress-responsive *cis*-acting elements ERSE, UPRE and ERSE-II. *J. Biochem.* **136**, 343–350 (2004).
9. D. Acosta-Alvear, Y. Zhou, A. Blais, M. Tsikitis, N. H. Lents, C. Arias, C. J. Lennon, Y. Kluger, B. D. Dynlacht, XBP1 controls diverse cell type- and condition-specific transcriptional regulatory networks. *Mol. Cell* **27**, 53–66 (2007).
10. I. Tabas, D. Ron, Integrating the mechanisms of apoptosis induced by endoplasmic reticulum stress. *Nat. Cell Biol.* **13**, 184–190 (2011).
11. H. Urra, E. Dufey, F. Lisbona, D. Rojas-Rivera, C. Hetz, When ER stress reaches a dead end. *Biochim. Biophys. Acta* **1833**, 3507–3517 (2013).
12. J. Soboloff, B. S. Rothberg, M. Madesh, D. L. Gill, STIM proteins: Dynamic calcium signal transducers. *Nat. Rev. Mol. Cell Biol.* **13**, 549–565 (2012).
13. S. H. Back, K. Lee, E. Vink, R. J. Kaufman, Cytoplasmic IRE1α-mediated *XBP1* mRNA splicing in the absence of nuclear processing and endoplasmic reticulum stress. *J. Biol. Chem.* **281**, 18691–18706 (2006).
14. D. Prins, J. Groenendyk, N. Touret, M. Michalak, Modulation of STIM1 and capacitative Ca^{2+} entry by the endoplasmic reticulum luminal oxidoreductase ERp57. *EMBO Rep.* **12**, 1182–1188 (2011).
15. L. Kantor, D. Pinchasi, M. Mintz, Y. Hathout, A. Vanderver, O. Elroy-Stein, A point mutation in translation initiation factor 2B leads to a continuous hyper stress state in oligodendroglial-derived cells. *PLOS One* **3**, e3783 (2008).
16. J. A. Vekich, P. J. Belmont, D. J. Thuerauf, C. C. Glembotski, Protein disulfide isomerase-associated 6 is an ATF6-inducible ER stress response protein that protects cardiac myocytes from ischemia/reperfusion-mediated cell death. *J. Mol. Cell. Cardiol.* **53**, 259–267 (2012).
17. A. Heifetz, W. J. Lennarz, Biosynthesis of N-glycosidically linked glycoproteins during gastrulation of sea urchin embryos. *J. Biol. Chem.* **254**, 6119–6127 (1979).
18. H. Yoshida, T. Matsui, N. Hosokawa, R. J. Kaufman, K. Nagata, K. Mori, A time-dependent phase shift in the mammalian unfolded protein response. *Dev. Cell* **4**, 265–271 (2003).
19. K. Yamamoto, H. Yoshida, K. Kokame, R. J. Kaufman, K. Mori, Differential contributions of ATF6 and XBP1 to the activation of endoplasmic reticulum stress-responsive *cis*-acting elements ERSE, UPRE and ERSE-II. *J. Biochem.* **136**, 343–350 (2004).
20. M. Waser, N. Mesaeli, C. Spencer, M. Michalak, Regulation of calreticulin gene expression by calcium. *J. Cell Biol.* **138**, 547–557 (1997).
21. L. Meunier, Y. K. Usherwood, K. T. Chung, L. M. Hendershot, A subset of chaperones and folding enzymes form multiprotein complexes in endoplasmic reticulum to bind nascent proteins. *Mol. Biol. Cell* **13**, 4456–4469 (2002).
22. C. E. Jessop, R. H. Watkins, J. J. Simmons, M. Tasab, N. J. Bulleid, Protein disulphide isomerase family members show distinct substrate specificity: P5 is targeted to BiP client proteins. *J. Cell Sci.* **122**, 4287–4295 (2009).
23. C. Y. Liu, H. N. Wong, J. A. Schauerte, R. J. Kaufman, The protein kinase/endoribonuclease IRE1α that signals the unfolded protein response has a luminal N-terminal ligand-independent dimerization domain. *J. Biol. Chem.* **277**, 18346–18356 (2002).
24. H. Li, A. V. Korennykh, S. L. Behrman, P. Walter, Mammalian endoplasmic reticulum stress sensor IRE1 signals by dynamic clustering. *Proc. Natl. Acad. Sci. U.S.A.* **107**, 16113–16118 (2010).
25. J. Hollien, J. S. Weissman, Decay of endoplasmic reticulum-localized mRNAs during the unfolded protein response. *Science* **313**, 104–107 (2006).
26. D. Han, A. G. Lerner, L. Vande Walle, J. P. Upton, W. Xu, A. Hagen, B. J. Backes, S. A. Oakes, F. R. Papa, IRE1α kinase activation modes control alternate endoribonuclease outputs to determine divergent cell fates. *Cell* **138**, 562–575 (2009).
27. J. Hollien, J. H. Lin, H. Li, N. Stevens, P. Walter, J. S. Weissman, Regulated Ire1-dependent decay of messenger RNAs in mammalian cells. *J. Cell Biol.* **186**, 323–331 (2009).
28. H. Coe, M. Michalak, Calcium binding chaperones of the endoplasmic reticulum. *Gen. Physiol. Biophys.* **28 Spec No Focus**, F96–F103 (2009).
29. S. Behrman, D. Acosta-Alvear, P. Walter, A CHOP-regulated microRNA controls rhodopsin expression. *J. Cell Biol.* **192**, 919–927 (2011).
30. B. P. Lewis, C. B. Burge, D. P. Bartel, Conserved seed pairing, often flanked by adenosines, indicates that thousands of human genes are microRNA targets. *Cell* **120**, 15–20 (2005).
31. A. Grimson, K. K. Farh, W. K. Johnston, P. Garrett-Engele, L. P. Lim, D. P. Bartel, MicroRNA targeting specificity in mammals: Determinants beyond seed pairing. *Mol. Cell* **27**, 91–105 (2007).
32. M. Maragkakis, M. Reczko, V. A. Simossis, P. Alexiou, G. L. Papadopoulos, T. Dalamagas, G. Giannopoulos, G. Goumas, E. Koukis, K. Kourtis, T. Vergoulis, N. Koziris, T. Sellis, P. Tsanakas, A. G. Hatzigeorgiou, DIANA-microT web server: Elucidating microRNA functions through target prediction. *Nucleic Acids Res.* **37**, W273–W276 (2009).
33. N. Elefant, A. Berger, H. Shein, M. Hofree, H. Margalit, Y. Altuvia, RepTar: A database of predicted cellular targets of host and viral miRNAs. *Nucleic Acids Res.* **39**, D188–D194 (2011).
34. Z. Ouyang, M. P. Snyder, H. Y. Chang, SeqFold: Genome-scale reconstruction of RNA secondary structure integrating high-throughput sequencing data. *Genome Res.* **23**, 377–387 (2013).
35. J. P. Upton, L. Wang, D. Han, E. S. Wang, N. E. Huskey, L. Lim, M. Truitt, M. T. McManus, D. Ruggero, A. Goga, F. R. Papa, S. A. Oakes, IRE1α cleaves select microRNAs during ER stress to derepress translation of proapoptotic caspase-2. *Science* **338**, 818–822 (2012).
36. N. Chitnis, D. Pytel, J. A. Diehl, UPR-inducible miRNAs contribute to stressful situations. *Trends Biochem. Sci.* **38**, 447–452 (2013).
37. D. A. Rodriguez, S. Zamorano, F. Lisbona, D. Rojas-Rivera, H. Urra, J. R. Cubillos-Ruiz, R. Armisen, D. R. Henriquez, E. H. Cheng, M. Letek, T. Vaisar, T. Irrazabal, C. Gonzalez-Billault, A. Letai, F. X. Pimentel-Muinos, G. Kroemer, C. Hetz, BH3-only proteins are part of a regulatory network that control the sustained signalling of the unfolded protein response sensor IRE1α. *EMBO J.* **31**, 2322–2335 (2012).
38. R. C. Friedman, K. K. Farh, C. B. Burge, D. P. Bartel, Most mammalian mRNAs are conserved targets of microRNAs. *Genome Res.* **19**, 92–105 (2009).
39. E. M. Small, R. J. Frost, E. N. Olson, MicroRNAs add a new dimension to cardiovascular disease. *Circulation* **121**, 1022–1032 (2010).
40. A. K. Leung, P. A. Sharp, MicroRNA functions in stress responses. *Mol. Cell* **40**, 205–215 (2010).
41. R. Kulshreshtha, M. Ferracin, S. E. Wojcik, R. Garzon, H. Alder, F. J. Agosto-Perez, R. Davuluri, C. G. Liu, C. M. Croce, M. Negrini, G. A. Calin, M. Ivan, A microRNA signature of hypoxia. *Mol. Cell. Biol.* **27**, 1859–1867 (2007).
42. C. J. Marsit, K. Eddy, K. T. Kelsey, MicroRNA responses to cellular stress. *Cancer Res.* **66**, 10843–10848 (2006).
43. S. N. Bhattacharyya, R. Habermacher, U. Martine, E. I. Closs, W. Filipowicz, Relief of microRNA-mediated translational repression in human cells subjected to stress. *Cell* **125**, 1111–1124 (2006).
44. S. Vasudevan, Y. Tong, J. A. Steitz, Switching from repression to activation: MicroRNAs can up-regulate translation. *Science* **318**, 1931–1934 (2007).
45. M. V. Sokolov, I. V. Panyutin, R. D. Neumann, Unraveling the global microRNAome responses to ionizing radiation in human embryonic stem cells. *PLOS One* **7**, e31028 (2012).
46. G. Tan, Y. Shi, Z. H. Wu, MicroRNA-22 promotes cell survival upon UV radiation by repressing PTEN. *Biochem. Biophys. Res. Commun.* **417**, 546–551 (2012).
47. X. Zhang, X. Lu, Posttranscriptional regulation of miRNAs in the DNA damage response. *RNA Biol.* **8**, 960–963 (2011).
48. V. Tarasov, P. Jung, B. Verdoodt, D. Lodygin, A. Epanchintsev, A. Menssen, G. Meister, H. Hermeking, Differential regulation of microRNAs by p53 revealed by massively parallel sequencing: miR-34a is a p53 target that induces apoptosis and G1-arrest. *Cell Cycle* **6**, 1586–1593 (2007).
49. E. van Rooij, L. B. Sutherland, X. Qi, J. A. Richardson, J. Hill, E. N. Olson, Control of stress-dependent cardiac growth and gene expression by a microRNA. *Science* **316**, 575–579 (2007).
50. X. Li, J. J. Cassidy, C. A. Reinke, S. Fischboeck, R. W. Carthew, A microRNA imparts robustness against environmental fluctuation during development. *Cell* **137**, 273–282 (2009).
51. A. S. Flynt, E. J. Thatcher, K. Burkewitz, N. Li, Y. Liu, J. G. Patton, *miR-8* microRNAs regulate the response to osmotic stress in zebrafish embryos. *J. Cell Biol.* **185**, 115–127 (2009).
52. P. J. Belmont, W. J. Chen, D. J. Thuerauf, C. C. Glembotski, Regulation of microRNA expression in the heart by the ATF6 branch of the ER stress response. *J. Mol. Cell. Cardiol.* **52**, 1176–1182 (2012).

53. R. Bartoszewski, J. W. Brewer, A. Rab, D. K. Crossman, S. Bartoszewska, N. Kapoor, C. Fuller, J. F. Collawn, Z. Bebok, The unfolded protein response (UPR)-activated transcription factor X-box-binding protein 1 (XBP1) induces microRNA-346 expression that targets the human antigen peptide transporter 1 (TAP1) mRNA and governs immune regulatory genes. *J. Biol. Chem.* **286**, 41862–41870 (2011).
54. G. Lugli, J. Larson, M. E. Martone, Y. Jones, N. R. Smalheiser, Dicer and eIF2c are enriched at postsynaptic densities in adult mouse brain and are modified by neuronal activity in a calpain-dependent manner. *J. Neurochem.* **94**, 896–905 (2005).
55. N. R. Smalheiser, G. Lugli, microRNA regulation of synaptic plasticity. *Neuromolec. Med.* **11**, 133–140 (2009).
56. C. Hetz, E. Chevet, H. P. Harding, Targeting the unfolded protein response in disease. *Nat. Rev. Drug Discov.* **12**, 703–719 (2013).
57. J. Groenendyk, M. Michalak, A genome-wide siRNA screen identifies novel phosphoenzymes affecting Wnt/β-catenin signaling in mouse embryonic stem cells. *Stem Cell Rev.* **7**, 910–926 (2011).
58. H. Coe, J. Jung, J. Groenendyk, D. Prins, M. Michalak, ERp57 modulates STAT3 signaling from the lumen of the endoplasmic reticulum. *J. Biol. Chem.* **285**, 6725–6738 (2010).
59. A. Azzalini, R package "sn": The skew-normal and skew-t distributions (version 0.4–16) (2010); http://cran.r-project.org/web/packages/sn.
60. T. Schagat, A. Paguio, K. Kopish, Normalizing genetic reporter assays: Approaches and considerations for increasing consistency and statistical significance. *Cell Notes* **17**, 9–12 (2007).
61. S. A. Seidel, P. M. Dijkman, W. A. Lea, G. van den Bogaart, M. Jerabek-Willemsen, A. Lazic, J. S. Joseph, P. Srinivasan, P. Baaske, A. Simeonov, I. Katritch, F. A. Melo, J. E. Ladbury, G. Schreiber, A. Watts, D. Braun, S. Duhr, Microscale thermophoresis quantifies biomolecular interactions under previously challenging conditions. *Methods* **59**, 301–315 (2013).
62. S. H. Back, M. Schröder, K. Lee, K. Zhang, R. J. Kaufman, ER stress signaling by regulated splicing: IRE1/HAC1/XBP1. *Methods* **35**, 395–416 (2005).
63. R. E. Milner, S. Baksh, C. Shemanko, M. R. Carpenter, L. Smillie, J. E. Vance, M. Opas, M. Michalak, Calreticulin, and not calsequestrin, is the major calcium binding protein of smooth muscle sarcoplasmic reticulum and liver endoplasmic reticulum. *J. Biol. Chem.* **266**, 7155–7165 (1991).
64. N. Mesaeli, K. Nakamura, E. Zvaritch, P. Dickie, E. Dziak, K. H. Krause, M. Opas, D. H. MacLennan, M. Michalak, Calreticulin is essential for cardiac development. *J. Cell Biol.* **144**, 857–868 (1999).
65. C. Hetz, P. Bernasconi, J. Fisher, A. H. Lee, M. C. Bassik, B. Antonsson, G. S. Brandt, N. N. Iwakoshi, A. Schinzel, L. H. Glimcher, S. J. Korsmeyer, Proapoptotic BAX and BAK modulate the unfolded protein response by a direct interaction with IRE1α. *Science* **312**, 572–576 (2006).
66. S. Brenner, The genetics of *Caenorhabditis elegans*. *Genetics* **77**, 71–94 (1974).
67. Y. Kong, Btrim: A fast, lightweight adapter and quality trimming program for next-generation sequencing technologies. *Genomics* **98**, 152–153 (2011).
68. B. Langmead, C. Trapnell, M. Pop, S. L. Salzberg, Ultrafast and memory-efficient alignment of short DNA sequences to the human genome. *Genome Biol.* **10**, R25 (2009).
69. J. Jurka, V. V. Kapitonov, A. Pavlicek, P. Klonowski, O. Kohany, J. Walichiewicz, Repbase Update, a database of eukaryotic repetitive elements. *Cytogenet. Genome Res.* **110**, 462–467 (2005).
70. S. Griffiths-Jones, S. Moxon, M. Marshall, A. Khanna, S. R. Eddy, A. Bateman, Rfam: Annotating non-coding RNAs in complete genomes. *Nucleic Acids Res.* **33**, D121–D124 (2005).
71. A. Kozomara, S. Griffiths-Jones, miRBase: Integrating microRNA annotation and deep-sequencing data. *Nucleic Acids Res.* **39**, D152–D157 (2011).
72. K. D. Pruitt, T. Tatusova, W. Klimke, D. R. Maglott, NCBI Reference Sequences: Current status, policy and new initiatives. *Nucleic Acids Res.* **37**, D32–D36 (2009).
73. M. S. Boguski, T. M. Lowe, C. M. Tolstoshev, dbEST—Database for "expressed sequence tags". *Nat. Genet.* **4**, 332–333 (1993).
74. I. L. Hofacker, Vienna RNA secondary structure server. *Nucleic Acids Res.* **31**, 3429–3431 (2003).
75. M. D. Robinson, D. J. McCarthy, G. K. Smyth, edgeR: A Bioconductor package for differential expression analysis of digital gene expression data. *Bioinformatics* **26**, 139–140 (2010).
76. F. Xiao, Z. Zuo, G. Cai, S. Kang, X. Gao, T. Li, miRecords: An integrated resource for microRNA–target interactions. *Nucleic Acids Res.* **37**, D105–D110 (2009).
77. N. H. Tan Gana, A. F. Victoriano, T. Okamoto, Evaluation of online miRNA resources for biomedical applications. *Genes Cells* **17**, 11–27 (2012).
78. F. L. Ramsey, D. W. Schafer, *The Statistical Sleuth: A Course in Methods of Data Analysis* (Brooks/Cole, Cengage Learning, Boston, ed. 3, 2013), pp. xxiv, 760.
79. T. Anderson, D. Darling, Asymptotic theory of certain goodness of fit criteria based on stochastic processes. *Ann. Math. Stat.* **23**, 193–212 (1952).
80. F. Wilcoxon, Individual comparisons by ranking methods. *Biometrics Bull.* **1**, 80–83 (1945).

Acknowledgments: We thank the members of the Michalak laboratory for valuable comments and suggestions. We thank R. Maranchuk at the RNAi screening core in the Department of Medical Microbiology and Immunology, University of Alberta, for his expert technical help. We thank B. Hazes (University of Alberta) for help with the analysis of the RNAi screen data. We thank T. Pozzan (University of Padova) for invaluable help, suggestions, and critical analysis of the data. We thank G. Kozlov and K. Gehring (McGill University) for the generous gift of purified PDIA6. **Funding:** Supported by the Canadian Institutes of Health Research grants MOP-15291, MOP-15415, and MOP-53050 to M.M.; NIH grants DK042394, DK088227, HL052173, and HL057346 to R.J.K.; NIH grant AI083432 to Y.G.; the American Heart Association (12SDG12040188) to S.S.; FONDEF D11I1007, Ring Initiative ACT1109; Millennium Institute No. P09-015-F, the Alzheimer's Association FONDECYT No. 1140549, ECOS CONICYT C13S02, the Muscular Dystrophy Association, ALS Therapy Alliance, and CONICYT-EEUU collaboration grant USA2013-0003 to C.H.; FONDECYT No. 3130365 postdoctoral grant to D.R.-R.; CONICYT PhD fellowships to E. Dufey, H.U., and D.S.; 2013 GIST Systems Biology Infrastructure Establishment Grant to D.H.K.; Korean Ministry of Science, ICT, and Future Planning (the Women Scientist program, 2013R1A1A3A04006010) to S.-K.L.; Korean Ministry of Education (Basic Science Research Program 2013R1A1A2005836) to J.A.; Alberta Innovates-Health Solutions graduate student scholarship to Z.P.; Dissertation Fellowship from University of Alberta to M.J.M.; and Alberta Innovates-Health Solutions postdoctoral fellowship to E. Dudek. **Author contributions:** J.G. designed experiments, analyzed data, performed biochemical and cell biological analyses and siRNA screening and validation experiments, and wrote the paper; E. Dudek, K.B., E. Dufey, H.U., D.S., and D.R.-R. designed experiments, analyzed data, and performed experiments; Z.P., X.F., M.J.M., and L.K. designed experiments and performed bioinformatics and computational analyses; K.B. analyzed ORAI1-deficient cells; S.S. and Y.G. developed and characterized ORAI1-deficient cells; J.A. and D.H.K. provided reagents for *C. elegans* experiments; Y.L. performed *C. elegans* experiments; S.-K.L. designed experiments and wrote the manuscript; R.J.K. designed experiments and developed and characterized IRE1 research tools; L.K., C.H., and M.M. designed experiments, analyzed data, and wrote the manuscript. **Competing interests:** The authors declare that they have no competing interests. **Data availability:** Deep sequencing data have been deposited with the NCBI GEO Sequence Database, accession no. GSE57138.

Submitted 6 December 2013
Accepted 12 May 2014
Final Publication 10 June 2014
10.1126/scisignal.2004983
Citation: J. Groenendyk, Z. Peng, E. Dudek, X. Fan, M. J. Mizianty, E. Dufey, H. Urra, D. Sepulveda, D. Rojas-Rivera, Y. Lim, D. H. Kim, K. Baretta, S. Srikanth, Y. Gwack, J. Ahnn, R. J. Kaufman, S.-K. Lee, C. Hetz, L. Kurgan, M. Michalak, Interplay between the oxidoreductase PDIA6 and microRNA-322 controls the response to disrupted endoplasmic reticulum calcium homeostasis. *Sci. Signal.* **7**, ra54 (2014).

Science Signaling
AAAS

www.sciencesignaling.org/cgi/content/full/7/329/ra54/DC1

Supplementary Materials for

Interplay Between the Oxidoreductase PDIA6 and microRNA-322 Controls the Response to Disrupted Endoplasmic Reticulum Calcium Homeostasis

Jody Groenendyk, Zhenling Peng, Elzbieta Dudek, Xiao Fan, Marcin J. Mizianty, Estefanie Dufey, Hery Urra, Denisse Sepulveda, Diego Rojas-Rivera, Yunki Lim, Do Han Kim, Kayla Baretta, Sonal Srikanth, Yousang Gwack, Joohong Ahnn, Randal J. Kaufman, Sun-Kyung Lee, Claudio Hetz, Lukasz Kurgan, Marek Michalak*

*Corresponding author. E-mail: marek.michalak@ualberta.ca

Published 10 June 2014, *Sci. Signal.* **7**, ra54 (2014)
DOI: 10.1126/scisignal.2004983

The PDF file includes:

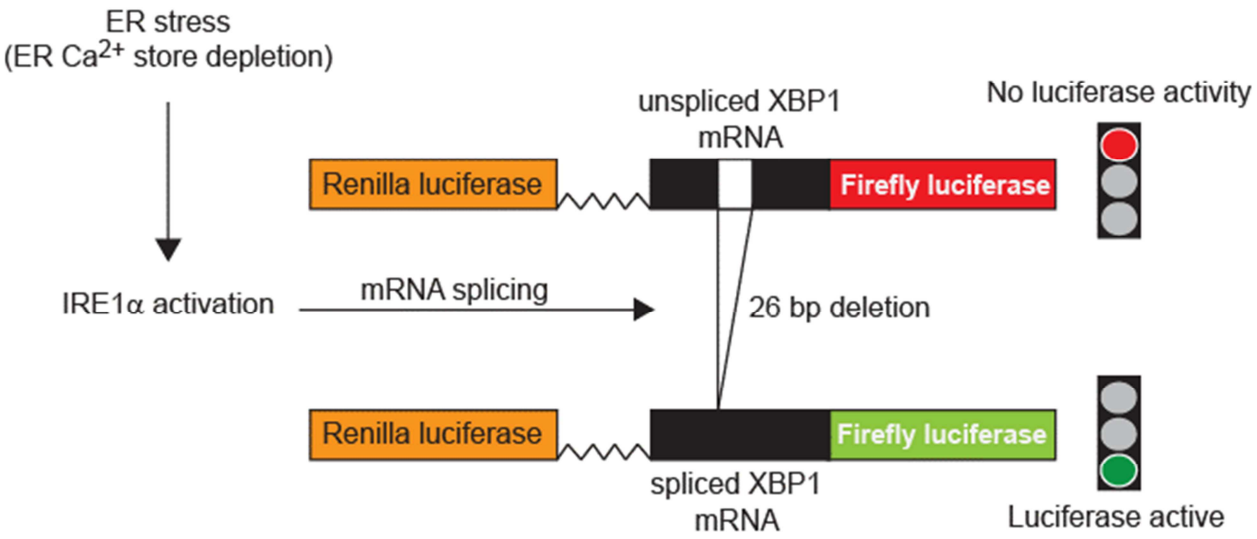

Supplemental Figure S1. The XBP1 splicing reporter system.
The pRL-IXFL XBP1 splicing reporter vector contained cDNA encoding Renilla luciferase (internal control) and cDNA encoding unspliced XBP1 followed by firefly luciferase. Because cDNA encoding the firefly luciferase is not in frame in the unspliced pRL-IXFL, there is no detectable luciferase activity. Induction of ER stress, specifically by ER Ca^{2+} store depletion, results in activation of the endoribonuclease activity of IRE1, which then splices 26 bp from the mRNA encoding XBP1. Splicing of the 26 bp fragment of the mRNA encoding XBP1 results in a frame shift that allows read through of the firefly luciferase enzyme.

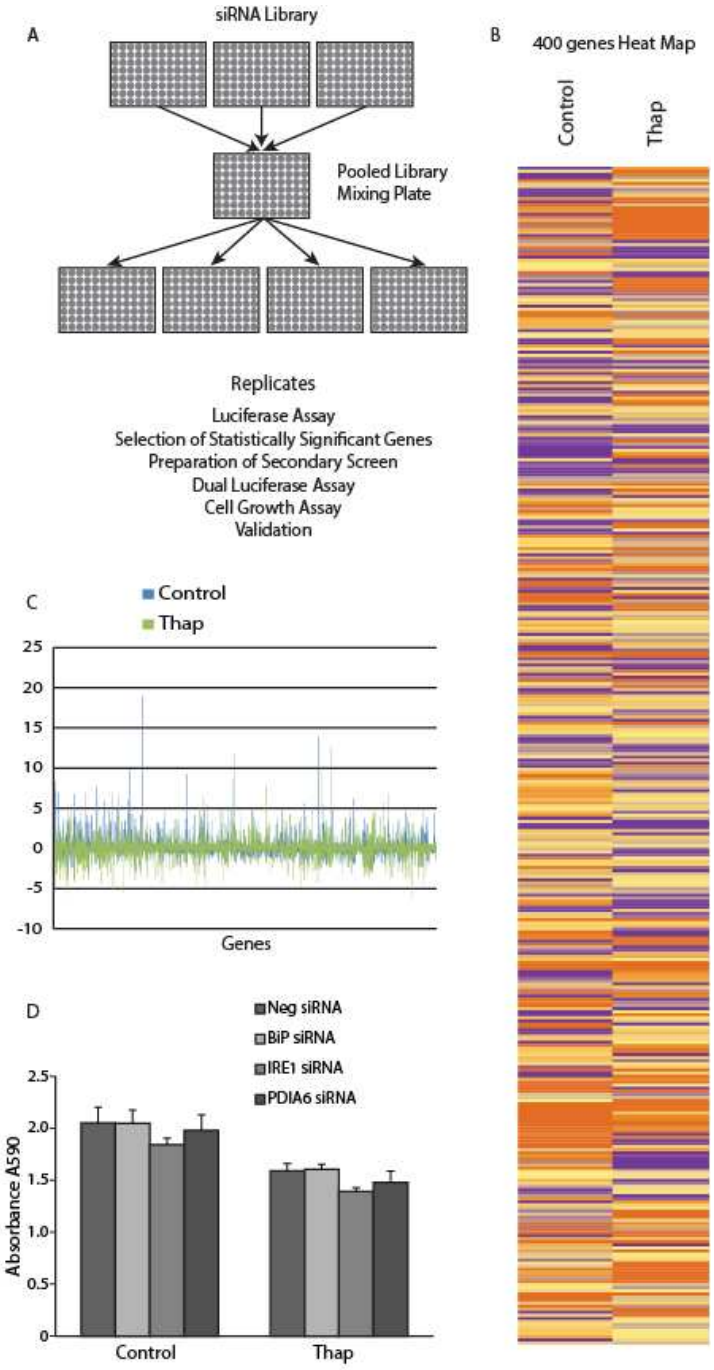

Supplemental Figure S2. A genome-wide siRNA screen.

(A). A schematic representation of the library screen. Transfection of single and pooled siRNA was performed in 24 well plates in duplicates in 3 independent experiments. qPCR for the selected high confidence genes was performed. (B). Heat maps representing 400 genes identified in control and thapsigargin (Thap)-treated cells. The cluster analysis is represented as a heat-map generated by Java TreeView 1.1.3. (C). A graph demonstrating the complete library screen. Y axis, fold change values. Thap, thapsigargin. (D). Cell growth of control and thapsigargin (Thap)-induced cells treated with siRNAs as indicated in the figure. Data is representative of 3 biological replicates.

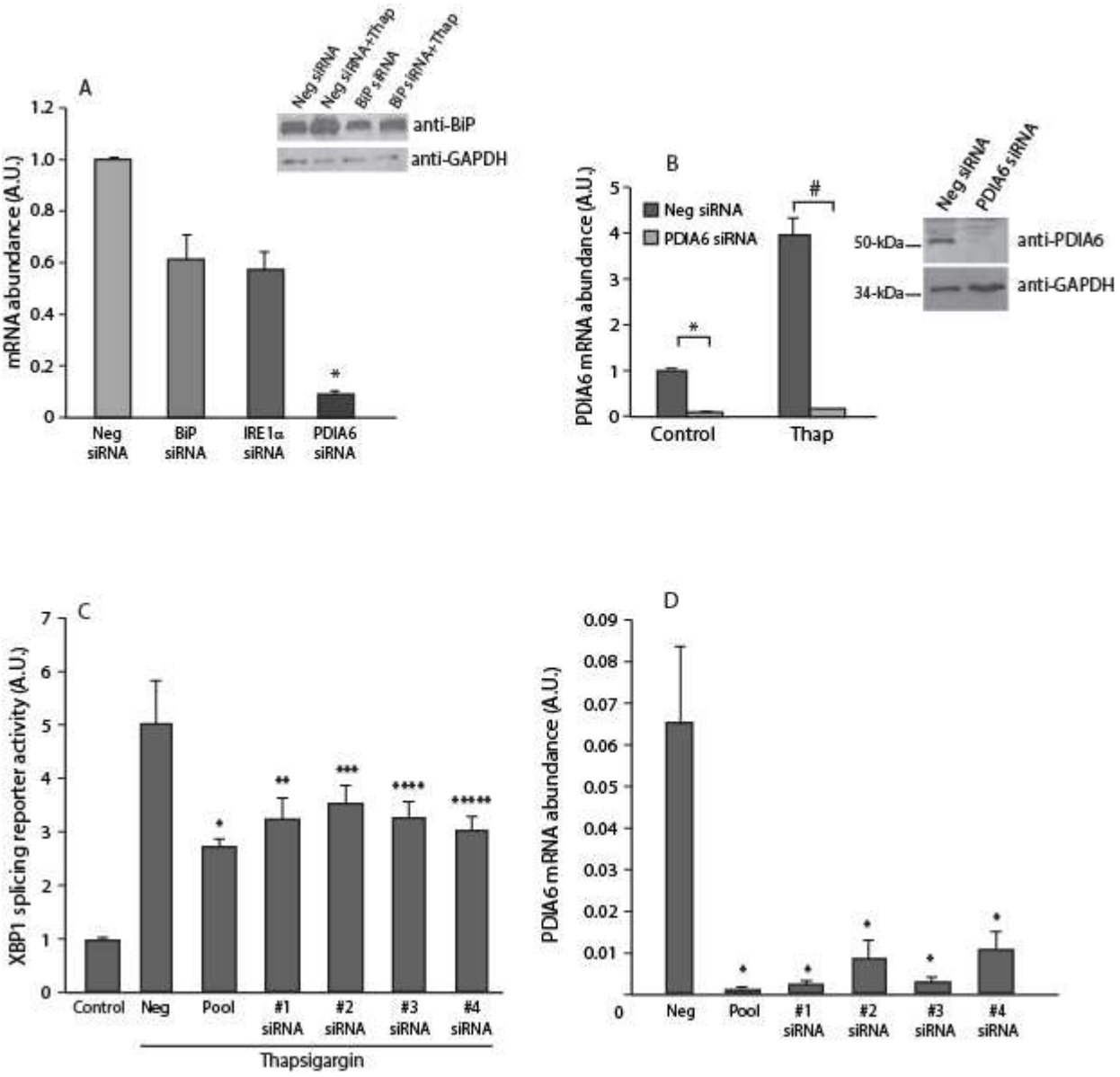

Supplemental Figure S3. Silencing of the PDIA6 gene.

(A). BiP, IRE1α, and PDIA6 genes were silenced using specific siRNA in NIH-3T3 cells expressing the IRE1α activity reporter. Scrambled, negative siRNA (control) was used as a control with results normalized to glyceraldehyde 3-phosphate dehydrogenase (GAPDH). *P-value = 4.11E-08. Inset, Western blot analysis with anti-BiP antibodies of control (Neg siRNA) and BiP siRNA treated cells. (B). Q-PCR analysis of PDIA6 mRNA abundance after silencing in the presence or absence of thapsigargin (Thap). Neg, negative scrambled control. Results were normalized to GAPDH. Control *P-value = 4.11E-08; thapsigargin #P-value = 4.48E-07. Inset, Western blot analysis with anti-PDIA6 antibodies of control and PDIA6 siRNA treated cells. Anti-GAPDH antibodies were used as a loading control. Data in (A) and (B) are representative of 3 or more biological replicates. (C). NIH-3T3 cells were transfected with XBP1 splicing reporter and either negative siRNA (Neg), pooled PDIA6 siRNA (pool), or four independent PDIA6-specific siRNA and treated with thapsigargin. *P-value <0.0001; **P-value = 0.0067; ***P-value

= 0.0069; ****P-value = 0.0016; *****P-value = 0.0005. (D). PDIA6 mRNA abundance in cells transfected with a different siRNA as shown in (C). *P-value <0.0001. Data in (C) and (D) is representative of 3 biological replicates.

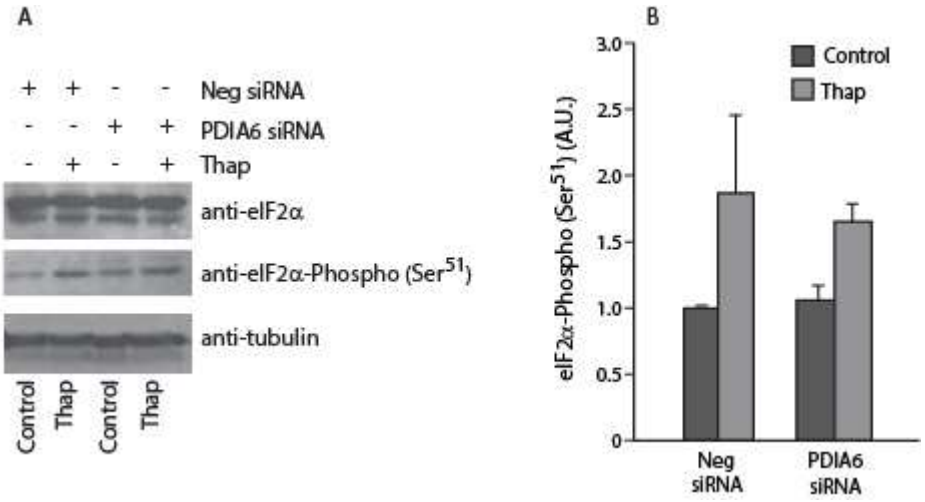

Supplemental Figure S4. Phosphorylation of eIF2α in PDIA6-silenced cells.
(A). PDIA6 was silenced in NIH-3T3 fibroblasts with siRNA. Cells were treated with thapsigargin (Thap) followed by Western blot analysis for total eIF2α (upper panel) and eIF2α phosphorylated at Ser^{51} (lower panel). (B). Quantitative analysis of phosphorylation of eIF2α at Ser^{51}. Thap, thapsigargin. Data in (A) and (B) are representative of at least 3 biological replicates.

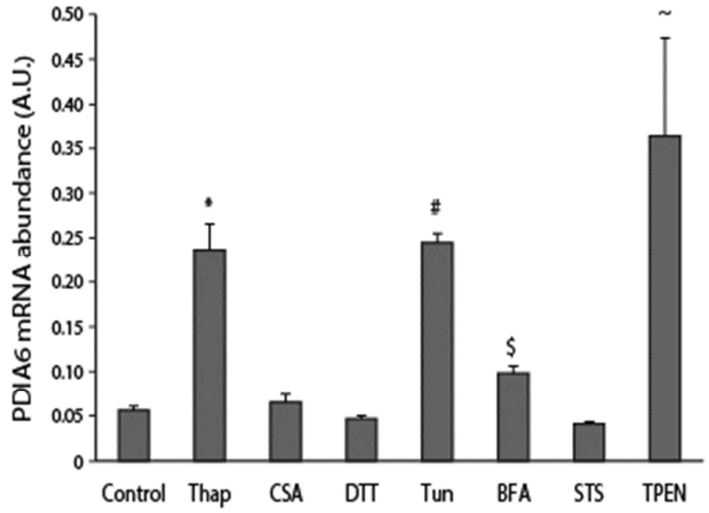

Supplemental Figure S5. PDIA6 mRNA abundance under ER stress conditions.
NIH-3T3 fibroblasts were treated with thapsigargin (Thap), cyclosporine A (CSA), dithiothreitol (DTT), tunicamycin (Tun), brefeldin A (BFA), staurosporine (STS) or tetrakis-(2-pyridylmethyl)ethylenediamine (TPEN). Results were normalized to the internal control GAPDH. *thapsigargin, P-value = 3.42E-13; #tunicamycin P-value = 1.54E-07; $brefeldin A P-value = 0.00126; ~TPEN P-value = 3.22E-05. All data are representative of at least 3 biological replicates.

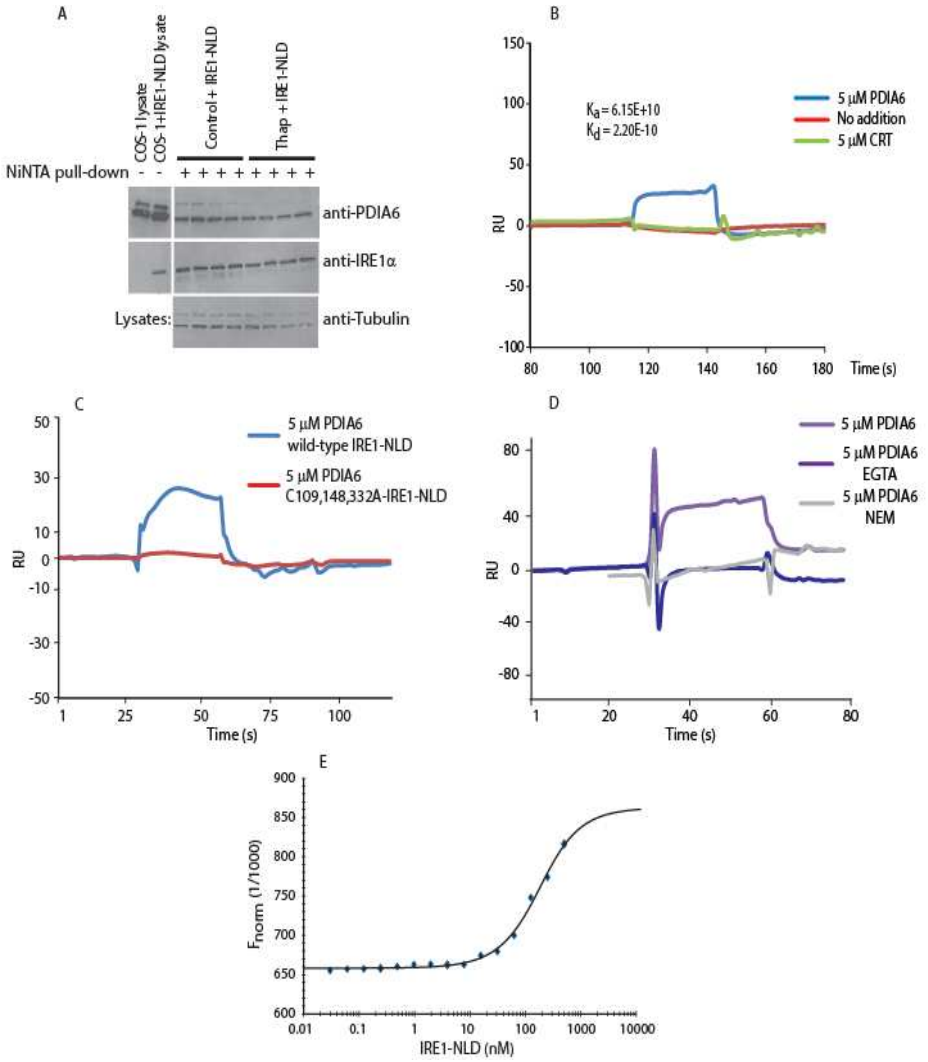

Supplemental Figure S6. PDIA6 interacts with the luminal domain of IRE1.
(A). His-tagged ER luminal domain of IRE1α (IRE1-NLD) was expressed in COS-1 cells. Four different pull-down experiments for control (Control + IRE1-NLD) and thapsigargin (Thap + IRE1-NLD) treated cells are presented. Total IRE1α and PDIA6 abundance in cell lysates is shown in the left panel. NiNTA, Ni-Agarose. (B). PDIA6 or calreticulin (CRT) was injected over immobilized recombinant IRE1α ER luminal domain (IRE1-NLD) coupled to a BIACore chip. RU, relative units. K_a and K_d values are representative of at least 3 independent biological replicates. (C). PDIA6 was injected over immobilized recombinant ER luminal domain of IRE1α (IRE1-NLD) or the triple cysteine mutant (C109A,C148A,C332A) of IRE1-NLD (C109,148,332A-IRE1-NLD) coupled to a BIACore chip. RU, relative units. K_a and K_d values are representative of at least 3 independent biological replicates. (D). PDIA6 was injected over immobilized recombinant IRE1α ER luminal domain in the presence of EGTA or after NEM-dependent alkylation of the coupled IRE1-NLD. RU, relative units. Graph is a representative of at least 3 independent biological replicates. (E). MST analysis of PDIA6 binding to IRE1-NLD. Graph is a representative of 3 independent biological replicates.

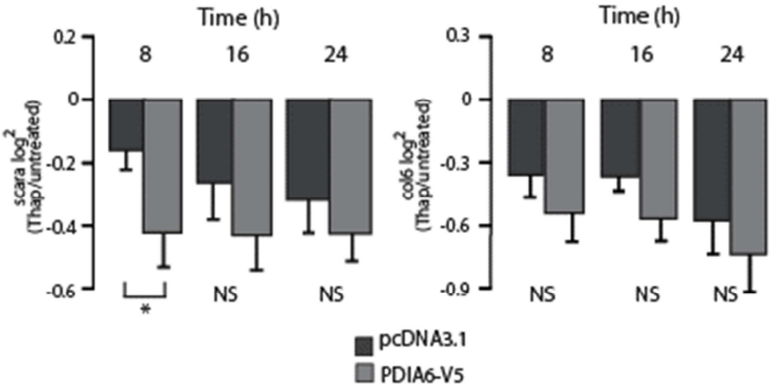

Supplemental Figure S7. PDIA6 silencing and IRE1α RIDD activity.
HEK293T cells were transiently transfected with PDIA6-V5 or control vector. mRNA decay (RIDD) of the IRE1α targets *scara* and *col6* was monitored by real-time PCR and normalized with respect to the abundance of the housekeeping gene *rpl19*. Data is representative of 3 independent biological replicates.

microRNA	Cont	Thap	Ratio T/C
mmu-miR-641-5p	43.5	3	0.068966
new_miRNA_star0666	42	3	0.0711429
mmu-miR-669f-3p	8.5	1	0.117647
mmu-miR-503	14.5	2	0.137931
mmu-miR-2137	25	6.5	0.26
mmu-miR-322	2127.5	665	0.312573
mmu-miR-708*	281	701.5	2.496441
new_miRNA0795	238	627	2.634454
mmu-miR-101b	954	2652	2.779874
mmu-miR-92a-1*	6.5	24.5	3.769231
mmu-miR-1937a	230.5	936	4.060738
new_miRNA_star0242	5.5	23.5	4.272727
new_miRNA0055	1.5	12.5	8.333333
mmu-miR-216b	1.5	13	8.666667
new_miRNA0056	1.5	27.5	18.33333
mmu-miR-216a*	1.5	28.5	19

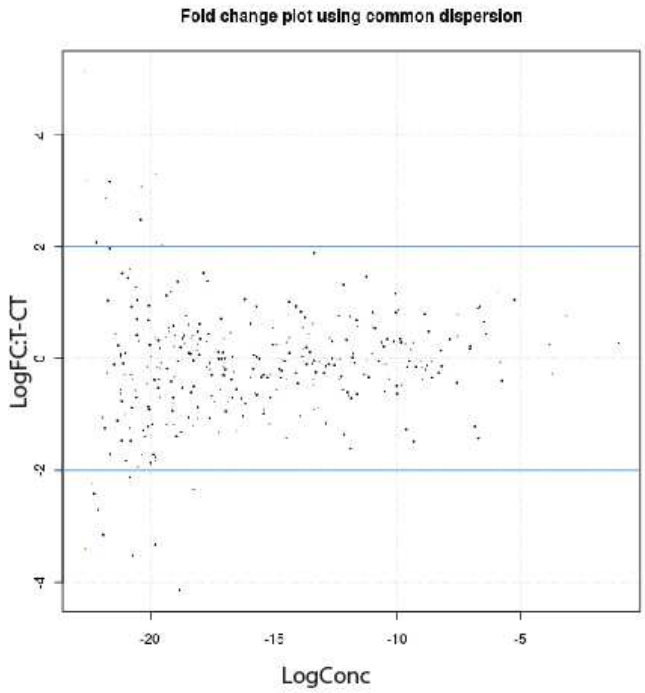

Supplemental Figure S8. Selected miRNAs identified by deep sequencing analysis.
Top table, high T/C (thapsigargin/control) ratio indicates thapsigargin-dependent increase in miRNA abundance and low T/C ratio indicates decrease in miRNA abundance, respectively. Lower panel, smear plot using fold change values of miRNA abundance with common dispersion. Log ratio compared to

abundance is presented. Data is representative of 2 independent biological replicates. Cont, control; Thap, thapsigargin.

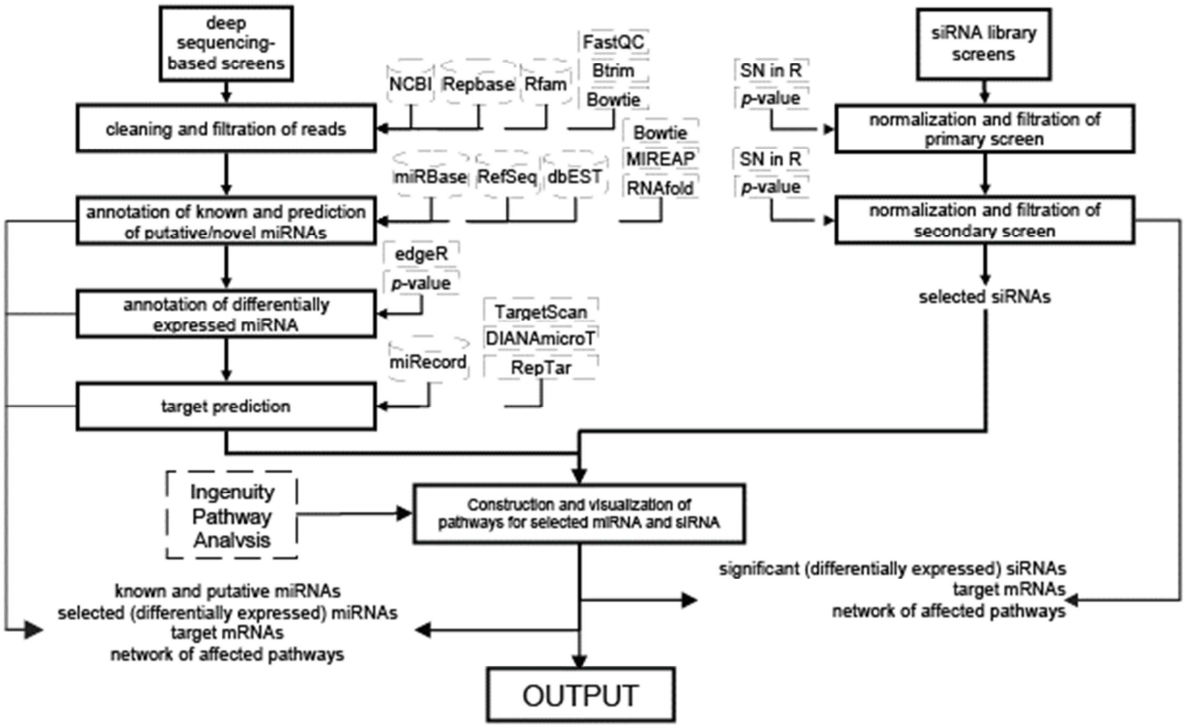

Supplemental Figure S9. Schematic representation of multiple target prediction analysis.
Outline of the computational analysis of the miRNA (on the left) and siRNA (on the right) screens. Black boxes denote main steps, dashed cylinders and boxes are databases and methods, respectively.